



TÉCNICO
LISBOA

Análise do Potencial da técnica “Additive Manufacturing”

Frederico Miguel Ferreira da Silva

Dissertação para a obtenção do grau de Mestre em

Engenharia de Materiais

Orientadores:

Prof. Doutor Maria Luísa Coutinho Gomes de Almeida

Prof. Doutor Maria de Fátima Reis Vaz

Júri

Presidente: Prof. Doutor Maria Amélia Martins de Almeida

Orientador: Prof. Doutor Maria de Fátima Reis Vaz

Vogais: Doutor Nuno Miguel Carvalho Pedrosa

Doutor Eurico Gonçalves Assunção

[Novembro de 2015]

I. Resumo

Os processos de fabrico do quotidiano estão altamente dependentes das operações de maquinação de modo a remover material até à forma final. Na indústria moderna são adoptadas todas as medidas que visem o fabrico de produtos de uma perspectiva sustentável, conciliando o baixo custo de fabrico e as questões ambientais.

Posto isto, a impressão 3D tem sido analisada duma perspectiva de industrialização, especialmente na produção de componentes metálicos. As técnicas de soldadura são chave na implementação dos processos de impressão 3D.

Fontes de potência como o laser e o feixe de electrões apresentam viabilidade para a fabricação aditiva de componentes mas na perspectiva de industrialização não são viáveis para fins industriais. Neste campo as tecnologias de soldadura por arco eléctrico apresentam sistemas já desenvolvidos e implementados na indústria como também possuem maior taxa de deposição comparativamente ao laser e ao feixe de electrões.

Neste trabalho, o processo GMAW foi usado devido ao facto de ser um processo usado largamente a nível industrial como pela sua eficiência e variantes existentes. O consumível usado na realização deste trabalho é designado por ER 5356, equiparado à liga de alumínio 5083. A variante estudada foi o *Cold Metal Transfer* que apresenta especial destaque em vários trabalhos na área da Fabricação Aditiva devido à capacidade de operar em regimes de baixa entrega térmica. A eficiência do depósito, entrega térmica, aproveitamento de material, dureza, metalografia e ensaios não destrutivos foram os aspectos estudados como indicadores do potencial da fabricação aditiva.

II. Palavras-chave

Impressão 3D, Fabricação Aditiva, CMT (Cold Metal Transfer), Liga de Alumínio 5083, Eficiência de deposição, metalografia.

III. Abstract

Nowadays the manufacturing processes are highly dependent on the machining operations to remove material up to the final shape. In modern industry are taken all measures to manufacture products in a sustainable perspective, combining the low manufacturing cost and environmental issues in account.

Therefore, 3D printing has been analyzed from a perspective of industrialization, especially in the production of metallic components. The welding techniques are the key solution in implementing 3D printing processes.

Power sources such as laser and electron beam were feasible for the additive manufacturing but in the perspective of industrialization are not viable. In this field, electric arc welding technology systems have been developed and implemented in industry long ago and also present higher deposition rates compared to laser and electron beam power sources.

In this work, the GMAW process was used due to the fact that it is a process widely used industrially as for its efficiency and existing variants. The consumable used in this work is ER 5356, equivalent to the 5083 aluminum alloy. The variant studied was Cold Metal Transfer (CMT) presenting special emphasis in several works in the field of Additive Manufacturing due to the ability to operate with low heat input. Deposition of efficiency, heat input, useful material ratio, hardness, metallographic and nondestructive testing were the aspects studied as indicators of potential analysis for additive manufacturing.

IV. Keywords

3D Printing, Additive Manufacturing, CMT (Cold Metal Transfer), Aluminium alloy 5083, Deposition efficiency, metallography.

V. Agradecimentos

A realização deste trabalho não seria possível sem a colaboração de diversas pessoas e entidades, às quais eu desejo os meus mais sinceros agradecimentos.

À Professora Luísa Coutinho, a orientadora deste trabalho, agradeço toda a solicitude e confiança depositada em mim, mostrando-se sempre disponível em solucionar todas as questões e dificuldades no decorrer do trabalho numa forma consistente e incansável.

Agradeço à Professora Maria de Fátima Reis Vaz por todo o apoio e interesse demonstrado no decorrer dos trabalhos, essencialmente nos testes metalográficos e na análise microscópica.

Agradeço ao Doutor Eurico Assunção pela total disponibilidade e abertura na discussão dos mais diversos problemas operatórios e teóricos como na solução dos mesmos, recorrendo ao seu *know-how* e experiência prévia.

Um agradecimento especial ao Doutor Filipe Nascimento agradeço a amizade e solicitude com que me acolheu na rotina na STM e me aconselhou durante todo o decorrer da dissertação, mostrando-se um pilar importante na realização deste trabalho.

Agradeço ao Doutor Nuno Pedrosa e ao Engenheiro António Sá Nogueira, da parte do LABEND do ISQ, por toda a disponibilidade na realização de ensaios não destrutivos e sua apreciação nos aspectos de inspeção.

Agradeço ao Doutor Carlos Silva e ao Senhor Farinha por toda a ajuda nas tarefas de laboratório, desde a preparação dos ensaios até à resolução de entraves técnicos no decorrer do trabalho.

Agradeço ao senhor Afonso Moutinho, por toda a ajuda e disponibilidade na resolução de problemas e elaboração dos procedimentos operativos no sistema robotizado.

Agradeço à Ana Beatriz Galvanito pela amizade e preciosa ajuda no tratamento de imagem dos ensaios macrográficos.

Agradeço aos meus colegas e amigos António Sá Nogueira, Ricardo Novais, João Marques, Ricardo Pedro, Rui Rodrigues, Tiago Matos, Teresa Laranjeira, Maria Ana Neves, Daniel Pimentel e Maria Inês Cunha pela amizade e apoio dado não só no decorrer da dissertação, mas também no decorrer do curso. O apoio e amizade incondicionais foram sem dúvida uma força motriz na conclusão do curso.

Agradeço aos meus amigos exteriores ao Instituto Superior Técnico, Tiago Ferreira, André Luz, Diogo Luz, André Candeias, Jorge Carvalho, Catarina Santos, Bruno Santos, Filipa Braz e Miguel Brito Costa, por toda a força transmitida em todos os momentos, especialmente na realização deste trabalho que representa um marco importante na minha carreira académica.

Agradeço à família Fonseca, Cesário, Hermínia e Joana, por todo o aconselhamento e apoio dado, que sem dúvida foram cruciais no decorrer do trabalho.

Por fim, agradeço à minha família por tudo o que eu sou e me tornei, não esquecendo um especial agradecimento especial à minha irmã, futura Mestre Sara Silva, a principal razão de hoje ser aluno do curso de Engenharia de Materiais nesta casa que é o Instituto Superior Técnico e por me ter guiado por etapas mais complicadas no decorrer desta jornada fantástica, que é encerrada com este trabalho.

VI. Acknowledgments

This work would not be possible to complete without the collaboration of several people and entities, which I manifest my sincere thanks.

To Professor Luísa Coutinho, the main guidance teacher of this work, I thank all the concern and the trust deposited in my person, and for being always available to solve all questions and difficulties during the work, in a consistent and unwearing way.

I thank to Professor Maria de Fátima Reis Vaz for all the support and interest during all work, especially on metallographic tests and its microscopic analysis.

I also would like to thank to Doctor. Eurico Assunção by the availability and openness for discussion of the several operative and theoretical problems as the solution for them, using its know-how and previous experience.

Special thanks to Doctor Filipe Nascimento, I appreciate the friendship, the warm welcome into the routine in STM and the advisement during this work , being an important pillar in this work.

Many thanks to Doctor Nuno Pedrosa and Engineer António Sá Nogueira, from LABEND of ISQ, the availability of performing the non-destructive tests and their evaluation in the inspection issues.

I would like to thank Doctor Carlos Silva and Mr. Farinha for all the help in the tasks required for this work, from the preparation to troubleshooting of technical difficulties.

Also want to thank Mr. Afonso Moutinho for all the help and availability on the procedures and troubleshooting with the robot system.

I thank to my friend Ana Beatriz Galvanito, for the friendship and the precious help on the image processing and editing for macro structure analysis.

I thank to my colleagues and friends António Sá Nogueira, Ricardo Novais, João Marques, Ricardo Pedro, Teresa Laranjeira, Maria Ana Neves, Daniel Pimentel e Maria Inês Cunha for their friendship and support not just through this work, but also the entire course. The unconditional friendship and support were definitely a driving force on the conclusion of the course.

Also for my friends outsider Instituto Superior Técnico, Tiago Ferreira, André Luz, Diogo Luz, André Candeias, Jorge Carvalho, Catarina Santos, Bruno Santos , Filipa Braz and Miguel Brito Costa for all the strength transmitted in all moments, especially in the execution of this work that represents an important milestone in my academic career.

I thank to Fonseca family, Cesário, Hermínia and Joana, for all the advisement and support given, no doubt that they were essential through the work execution.

At last, I thank to my family for all that I am and I have become, not forgetting a special thanks for my sister, future Master Sara Silva, the main reason for me to be a Materials Engineer student in this institution that is Instituto Superior Técnico and for the guidance through all rough stages during this fantastic journey, which is marked with this work.

VII. Index

Contents

I.	Resumo	i
II.	Palavras-chave	i
III.	Abstract	ii
IV.	Keywords	ii
V.	Agradecimentos.....	iii
VI.	Acknowledgments	v
VII.	Index	vii
VIII.	List of Figures	ix
IX.	List of Tables	xii
X.	List of Acronyms	xiii
1.	Introduction.....	1
1.1.	Motivation	1
1.2.	Objectives	1
1.3.	Structure of the work	1
2.	Literature review	3
2.1.	Metallic Additive Manufacturing (MAM) processes.....	6
2.1.1.	Electron Beam Additive Manufacturing (EBAM)	8
2.1.2.	Laser Additive Manufacturing (LAM)	9
2.1.3.	Wire and Arc Additive Manufacturing (WAAM).....	12
2.2.	Metal Additive Manufacturing Summary	16
2.3.	Aluminium	17
2.3.1.	Properties and Applications	17
2.3.2.	Production	17
2.3.3.	Alloy designation and treatments	19
2.4.	Gas Metal Arc Welding	19
2.4.1.	Short-circuiting transfer	20
2.4.2.	Pulsed Arc Transfer.....	21
2.4.3.	Globular Transfer	21
2.4.4.	Spray Transfer.....	22
2.4.5.	Cold Metal Transfer (CMT)	23
2.5.	Literature review summary	24
3.	Experimental Procedure	25

3.1. Layer by layer wall building	25
3.2. Current and Voltage Data Acquisition	28
3.3. Deposition Efficiency and Heat Input calculation.....	29
3.4. Non Destructive Testing	30
3.5. Macrostructure and microstructure analysis	34
3.5.1. Macrostructure analysis	35
3.5.2. Microstructure analysis	36
3.6. Hardness.....	36
4. Results and Discussion.....	38
4.1. Deposition Efficiency and Heat Input	38
4.1.1. Wall build up.....	38
4.1.2. Voltage and Current average calculations.....	39
4.1.3. Deposition Efficiency and Heat Input	42
4.2. Macrostructure Analysis.....	45
4.3. Hardness.....	48
4.4. Microstructure analysis	50
4.5. Non Destructive Testing	55
4.5.1. Phased Array Ultrasound Testing	55
4.5.2. Pulsed echo Ultrasound Testing and Radiation Testing	58
5. Conclusions.....	65
6.Future work.....	66
XI. References	67
XII. Appendixes	73
Appendix A: Technical Specification Sheet of Filler wire ER5356.....	74
Appendix B: Experimental Procedure for Metallographic analysis	75
Appendix B1: Experimental procedure for Macrostructure and analysis	75
Appendix B2: Experimental procedure for Microstructure and analysis	76
Appendix C: Experimental Procedure for Hardness testing	77
Appendix C1: Values obtained of Hardness testing	77

VIII. List of Figures

Figure 2.1: Additive Manufacturing process flowchart [4].....	4
Figure 2.2: Total fly and buy weight in million pounds for (a) airframes and (b) aero engines production. Buy weight figures exclude the recycling operations, representing the Buy to Fly ratio [7]	5
Figure 2.3: Relation between Cost per assembly vs. Production volume comparing Selective Laser Sintering (SLS) and High Production Die casting (HPDC) [5].....	5
Figure 2.4: Relation between cost per part and complexity [4]	5
Figure 2.5: Schematic representation of Layer Manufacturing (LM) for metals [20].....	6
Figure 2.6: Representation of a powder nozzle feeding system [18]	7
Figure 2.7: Representation of a powder bed feeding system [18]	7
Figure 2.8: Representation of a wire feeding system [18]	7
Figure 2.9: Representative scheme of the EBAM process [25]	8
Figure 2.10: Parts manufactured by EBAM process [26].....	9
Figure 2.11: Aluminium functional part manufactured by SLS process [37]	10
Figure 2.12: Metallic structure fabricated by SLM process [38].....	10
Figure 2.13: Manufactured part and processing using LENS technology [39].....	10
Figure 2.14: Representative scheme of the SLM/SLS process [9]	11
Figure 2.15: Representative scheme of the LENS process [44]	12
Figure 2.16: Tubular Ti-6Al-4V components made by WAAM processes [42]	13
Figure 2.17: WAAM manufactured part before machining (left) and after machining (right) [39]	13
Figure 2.18: Representative scheme of the GTAW process [54]	14
Figure 2.19: Representative scheme of the Plasma Additive Manufacturing [47]	14
Figure 2.20: Representative scheme of GMAW [54].....	15
Figure 2.21: Representative scheme of the CMT operation cycle [55]	15
Figure 2.22: Aluminium elaboration process [98]	18
Figure 2.23: Aluminium alloy series and its heat and mechanical treatments [98]	19
Figure 2.24: Cycle duty of short circuiting transfer [52].....	20
Figure 2.25: Pulsed transfer mechanism representing Current vs. Time [99].....	21
Figure 2.26: Globular transfer scheme in GMAW process [52]	22
Figure 2.27: GMAW Spray transfer schematic [101]	22
Figure 2.28: CMT operation cycle.....	23
Figure 2.29: Current and voltage variation through time in a single CMT operation cycle [102]	23
Figure 3.1: Fronius CMT VR 7000	25
Figure 3.2: Kuka 6-axis robot.....	25
Figure 3.3: Fronius parameter controller RCU 5000i.....	26
Figure 3.4: National Instruments DAQ device	26
Figure 3.5: Current transducer LEM LT 500-S.....	26
Figure 3.6: Tension transducer LEM CV 3-200/SP6	26
Figure 3.7: Wall build up first iteration	26
Figure 3.8: Wall build up second iteration	27
Figure 3.9: travelling process and signal acquisition regarding the existence of defects [103]	31
Figure 3.10: Huygens principle represented in the Phased Array UT [104].	31
Figure 3.11: Surface of the plate used for the analysis, for both procedures	33
Figure 3.12: Experimental procedure equipment for the Phased Array test, where the plate it is submerged and the scanning probe is coupled with the automated system.	33
Figure 3.13: Trajectory made by the sound probe in the Phased Array UT	33
Figure 3.14: Experimental setup for the radiation NDT	34

Figure 3.15: Hardness test principle illustration.....	36
Figure 4.1: Test part 130A	38
Figure 4.2: Test part 120A	38
Figure 4.3: Test part 110A	38
Figure 4.4: Test part 100A	38
Figure 4.5: Test part 90A	39
Figure 4.6: Test part 80A	39
Figure 4.7: Test part 70A	39
Figure 4.8: Test part 60A	39
Figure 4.9: Waveform for current in CMT operation cycle for 90A sample	39
Figure 4.10: Voltage Waveform in CMT operation cycle for 90A sample	40
Figure 4.11: Calibration coefficient for Current DAQ	41
Figure 4.12: Calibration coefficient for Voltage DAQ	41
Figure 4.13: Relation between Wire Feeding Rate and current	42
Figure 4.14: Relation between the number of layers and heat input	43
Figure 4.15: Graphic relation between Deposition Efficiency and Heat Input	44
Figure 4.16: Relation between Deposition Efficiency and Heat Input.....	44
Figure 4.17: Useful area represented for parts 130A, 110A, 80A and 60 A respectively	45
Figure 4.18: Relation between UMR and the number of layers.....	46
Figure 4.19: Relation between UMR and the Deposition Efficiency	46
Figure 4.20: Relation between UMR and Heat Input	47
Figure 4.21: Relation between UMR and Weight of electrode used.....	47
Figure 4.22: Hardness test patterns applied in all test part sections	48
Figure 4.23: Hardness distribution along the section of 130A test part	49
Figure 4.24: Hardness distribution along the section of 110A test part	49
Figure 4.25: Hardness distribution along the section of 80A test part.....	49
Figure 4.26: Hardness distribution along the section of 60A test part.....	50
Figure 4.27: SEM image captured from the 130A test part with 1000x magnification	51
Figure 4.28: SEM image captured from the 130A test part with 3000x magnification	51
Figure 4.29: SEM image captured from the 110A test part with 1000x magnification	51
Figure 4.30: SEM image captured from the 110A test part with 3000x magnification	51
Figure 4.31: SEM image captured from the 80A test part with 1000x magnification	51
Figure 4.32: SEM image captured from the 80A test part with 3000x magnification	51
Figure 4.33: SEM image captured from the 60A test part with 1000x magnification	52
Figure 4.34: SEM image captured from the 60A test part with 3000x magnification	52
Figure 4.35: 130A test part microstructure with 50x magnification.	53
Figure 4.36: 110A test part microstructure with 50x magnification.	53
Figure 4.37: 80A test part microstructure with 50x magnification.	53
Figure 4.38: 80A test part microstructure with 50x magnification.	53
Figure 4.39: 130A test part with 3000x magnification with the pores highlighted	54
Figure 4.40: 110A test part with 3000x magnification with the pores highlighted	54
Figure 4.41: 80A test part with 3000x magnification with pores highlighted	54
Figure 4.42: 60A test part with 3000x magnification with the pores highlighted	54
Figure 4.43: AM steel parts with the respective indication number	56
Figure 4.45: Multi 2000 software display	56
Figure 4.46: Steel parts for NDT testing numbered from 1 to 7	59
Figure 4.47: UT spectre for the steel test vs. X-Ray part 1	60
Figure 4.48: UT spectre for the steel test vs. X-Ray part 2	60
Figure 4.49: UT spectre for the steel test vs. X-Ray part 3	61
Figure 4.50: UT spectre for the steel test vs. X-Ray part 4	61

Figure 4.51: UT spectre for the steel test vs. X-Ray part 5	62
Figure 4.52: UT spectre for the steel test vs. X-Ray part 6	62
Figure 4.53: UT spectre for the steel test vs. X-Ray part 7	63
Figure 4.54: UT spectre for the Aluminium test vs. X-Ray part 1A	64

IX. List of Tables

Table 2.1: Analysis of different additive manufacturing processes.....	16
Table 2.2: Publications made on AM regarding only the materials used	16
Table 3.1: Initial parameter setting defined for wall buildings	27
Table 3.2: Advantages and limitations of UT.....	30
Table 4.1: Parameters obtained for each test part	42
Table 4.2: Deposition efficiency and weights used for its determination	42
Table 4.3: Heat Input values and parameter used for its determination	43
Table 4.4: UMR calculations and values used for its calculation.....	45
Table 4.5: Average Hardness of each test part.....	50
Table 4.6: Chemical composition obtained in the EDS analysis, for each test part, concerning the zones of interest.	52
Table 4.7: Average grain size for each test part	53
Table 4.8: Porosity analysis considering the occupied area and average size	54
Table 4.9: AM steel parts dimensions	55
Table 4.10: Summary table of the PAUT analysis	58
Table 4.11: AM steel part dimensions	59
Table 4.12: AM aluminium part dimensions	59
Table 4.13: X-Ray testing conditions and IQI obtained	59

X. List of Acronyms

AM – Additive manufacturing

MAM – Metal Additive Manufacturing

CMT – Cold Metal Transfer

GMAW – Gas Metal Arc Welding

GTAW – Gas Tungsten Arc Welding

PAW – Plasma Arc Welding

3D – Three Dimensional

RP – Rapid Prototyping

SL – Stereolithography

FDM – Fused Deposition Material

IJP – Ink Jet Printing

SLS – Selective Laser Sintering

SLM – Selective Laser Melting

LOM – Laminated Object Manufacturing

RM – Rapid Manufacturing

CAD – Computerized Assisted Design

CAM – Computerized Assisted Manufacturing

CNC – Computerized Numerical Control

BTF – Buy-to-fly

HPDC – High Production Die Casting

EBAM – Electron Beam Additive Manufacturing

LAM – Laser Additive Manufacturing

LENS – Laser Engineered Net Shaping

WAAM – Wire and Arc Additive Manufacturing

I – Current Intensity

V – Voltage

WFS – Wire Feeding Speed

TS – Travel speed

DC – Direct Current

AC – Alternate Current

GMAAM – Gas Metal Arc Additive Manufacturing

MIG – Metal Inert Gas

MAG – Metal Active Gas

DAQ – Data Acquisition

WEU – Weight of Eletrode Used

DE – Deposition Efficiency

HI – Heat Input

HV – Hardness Vickers

NDT – Non Destructive Testing

UT – Ultrasonic Testing

VI – Visual Inspection

LPT – Liquid Penetrant Testing

MPT – Magnetic Particle Testing

EC – Eddy Currents

UMR – Useful Mass Ratio

PAUT – Phased Array Ultrasonic Testing

A_e – Eletrode area

ρ_e – Eletrode density

t_w – Welding time

1. Introduction

1.1. Motivation

Additive manufacturing (AM) technologies are becoming increasingly important techniques in the fabrication of parts that includes a wide range of metals, polymers and composites used as raw material. However the main focus on the present work will be in metallic additive manufacturing.

Nowadays, automotive and aerospace industries seek solutions that allow the production of complex full density metal parts with low production batches, associated to good mechanical properties. There is a growing interest in the research and development in the metal additive manufacturing and its interest is related with the advantages associated with this process.

Metal Additive Manufacturing (MAM) can be classified by energy source, feeding system and deposition rate, in order to suit the desired application. Arc welding is suitable for most used metals and alloys and recently studied for AM purposes. The most used arc welding processes are Gas Metal Arc Welding (GMAW), Gas Tungsten Arc Welding (GTAW) and Plasma Arc Welding (PAW). Gas Metal Arc Welding is studied in particular due to its process variants, Cold Metal Transfer (CMT), which allows suiting the AM needs because of its intrinsic characteristics.

1.2. Objectives

The objectives of this work are:

- To study the influence of the Current Intensity on the AM process, concerning the deposition efficiency, hardness characteristics on the AM section parts and metallurgical properties;
- Introduce the Non Destructive Testing techniques in order to prove that they are viable on AM.

1.3. Structure of the work

The work is organized by chapters and each one of them correspond to every stage of the work.

In chapter 1 the motivation, objectives and structure of the work are expressed.

In chapter 2, a literature review of Additive Manufacturing techniques, Aluminium alloys, the alloy that is studied and the CMT welding process used for the practical work is made.

In chapter 3 the used experimental procedure is described along with the decisions about parameter choice and approaches in order to fulfil the objectives.

In chapter 4 the results obtained in the experimental work are described.

Chapter 5 makes the discussion of the results obtained.

In chapter 6 the conclusions and future work are expressed.

2. Literature review

Additive Manufacturing (AM) is a fabrication method which consists on overlapping successive layers of material. The output is a three dimensional (3D) finished or near finished part. This manufacturing method does not appear in the history as that, but instead, it is introduced as a Rapid Prototyping (RP) process in the 1980's, with the objective of creating models of parts [1]. In this work the AM processes addressed regard metallic materials since the use of AM technologies for producing metal parts is growing rapidly and migrating from a technique used for manufacturing parts in high value raw materials, such as titanium and its alloys, to other materials as aluminium, steel and respective alloys. With this evolution, the manufacturing technologies used in AM are also changing in comparison with conventional technologies as welding, with laser and electron beam. Nowadays, automotive and aerospace industries seek new manufacturing technologies in order to improve efficiency in the entire productive process. AM technologies have the objective to produce near net shape, fully dense complex metallic parts with functional capabilities, therefore, allowing to produce complex parts. The main potential of this technique is to process high value alloys such as: titanium, nickel, cobalt, aluminium, stainless and tool steels. The advantages in economic and environmental aspects are attractive because the energy spent to process some of these alloys (p.e., machining) can be reduced, so as the solid waste rate associated to the operations necessary for the final part manufacturing.

RP technologies were used merely to produce models, mainly by Stereolithography (SL), Fused Material Deposition (FDM), Ink Jet Printing (IJP), Selective Laser Sintering (SLS), and Laminated Object Manufacturing (LOM) [2]. Those models were built from scratch, layer by layer with dimensional precision. This approach rapidly evolved and the parts were manufactured with the purpose to be functional, so Rapid Prototyping was soon called Rapid Manufacturing (RM).

RM can be considered the manufacturing of ready to use parts using the AM technologies, guaranteeing the full use of the part during its life cycle, which means fulfilling the physical, mechanical and geometrical properties envisaged for performing its function [3].

Modern manufacturing industries seek more and more RM technologies in order to become more competitive to produce functional, complex and dimensionally accurate parts [4]. Automotive and aerospace industries are examples of industries that invest on AM technologies due its potential economic and environmental factors instead of using the traditional manufacturing methods such as casting, machining and forging. For each one of the processes, the manufacturing operations are exactly the same, and none of the AM processes existing nowadays were possible without the combination of three major improvements of science and engineering: CAD (Computer Assisted Design), CAM (Computer Assisted Manufacturing) and CNC (Computer Numerical Control). Thus, the general steps (Figure 2.1) to produce a part with an AM technology are:

1. Design Conceptualization;
2. CAD elaboration;
3. Conversion to a STL file;
4. Processing the part;
5. Finishing operations.

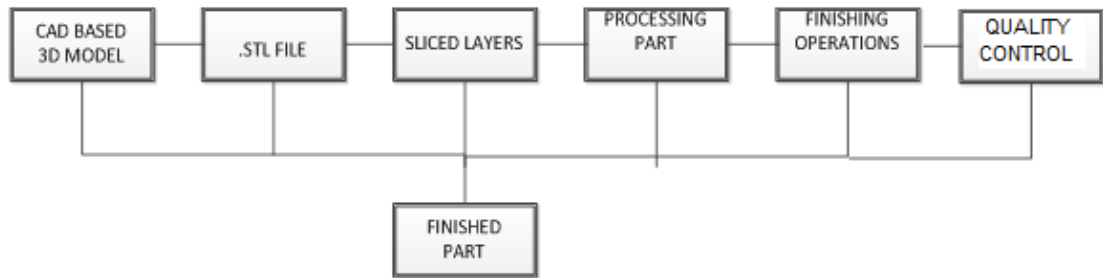


Figure 2.1: Additive Manufacturing process flowchart [4]

It is of general consensus that the AM processes bring the following benefits [5]:

- Tooling costs are reduced, reducing the time and cost on finishing operations
- The price per part barely varies, regardless of the amount of units on the production batch;
- It is possible to change design of the parts considering the functions of the part, allowing to optimize some aspects, for example the weight;
- There are no design restrictions, regarding the AM layer upon layer processing methods;
- It is economical favourable, considering the benefits above and the possibility to reduce waste,
- Finally, the inventories contain much less units.

In the aerospace industry, for example, the buy-to-fly ratio (BTF) (Figure 2.2) reflects the material efficiency of a manufactured component of traditional machining methods which present BTF ratios of 5:1, but in other cases, it can be greater than 20:1 [6], due to large amount of waste and difficult to recycle the material. Therefore, the need to develop new low-cost and more efficient manufacturing methods is critical to improve BTF ratios and to meet future sustainable manufacturing requirements.

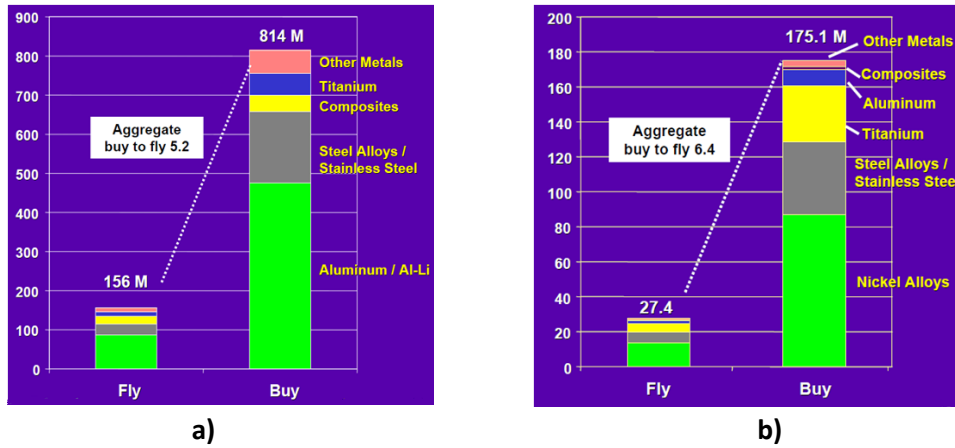


Figure 2.2: Total fly and buy weight in million pounds for (a) airframes and (b) aero engines production. Buy weight figures exclude the recycling operations, representing the Buy to Fly ratio [7]

When compared to traditional manufacturing processes, the AM technologies have a lower energy consumption, because the layer-by-layer manufacturing provide near net shape final parts, comparing to subtractive manufacturing technologies, like machining. AM has the upper hand because there is no need for a high amount of operations to fabricate [8].

The AM advantages compared with traditional manufacturing technologies are [9]:

- As a near net shaping process, the tooling costs are reduced as well the cost on personnel and equipment;
- The design complexity is not issue an issue, it allows to produce complex part and change its design without any extra cost, [10];
- It is economically favourable, because there is not as much raw material and energy consumption as the traditional methods [11] [19];
- The batches produced don't have a specific number of units avoiding numerous inventory units to be stored [12];
- The price per part hardly changes, disregarding the amount of units on the production batch [5] (Figures 2.3, 2.4).

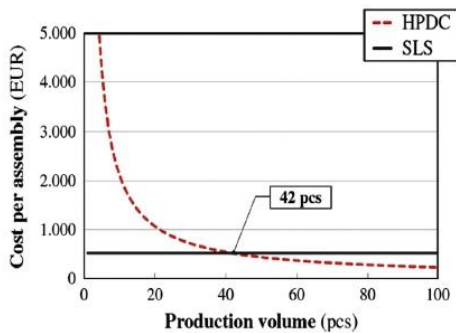


Figure 2.3: Relation between Cost per assembly vs. Production volume comparing Selective Laser Sintering (SLS) and High Production Die casting (HPDC) [5]

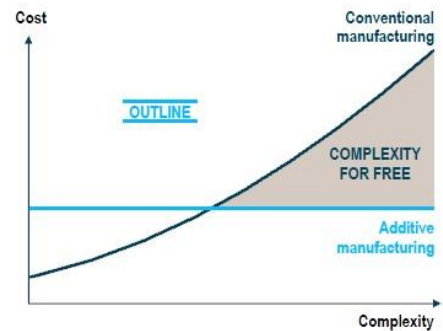


Figure 2.4: Relation between cost per part and complexity [4]

2.1. Metallic Additive Manufacturing (MAM) processes

In the last years RP systems and technology were developed and implemented in industry mostly for plastics. The next step was to develop those technologies in order to process other materials like metals, ceramics and to produce composite parts [13]. The existing literature on these types of materials is considerable. The metallic alloys are of interest for industries, like automotive, aerospace, military and medical, in particular to improve the manufacturing efficiency in processing high value metals [14].

The manufacturing of some metals is difficult and expensive so it is important to minimize the waste rate of the traditional processes [15] [16]. Metal Additive Manufacturing is a technique that can produce 3D parts with the main advantage that allows skipping some steps in the manufacturing process. The main concern of the use of MAM technologies is to guarantee that the final properties of the part produced are as good as the base material and that the required dimensional requirements are fulfilled.

The AM processes can be classified regarding its characteristics such as: feeding system, energy source and deposition rate (Figure 2.5) [17]. [18] [19].

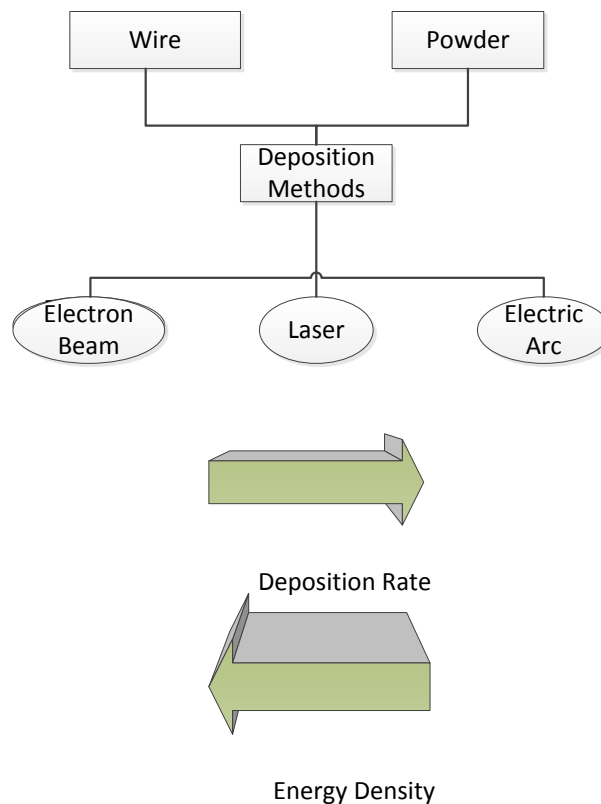


Figure 2.5: Schematic representation of Layer Manufacturing (LM) for metals [20]

The use of powder raw materials is more popular with Laser and Electron Beam energy sources, with two widely used systems: the powder bed system (Figure 2.7) and direct powder feeding system (Figure 2.6). In powder bed systems, a focused laser/electron beam travels across the surface of a metallic powder bed and selectively heats and fuses layers of consecutive cross sections according to the CAD model, until a part is finished. On the direct powder or wire feeding (Figure 2.6 and 2.8), there must be two independent systems: the heat source and the feeding system. The particularity in powder and wire feeding, the feeding is directly in the melting pool.

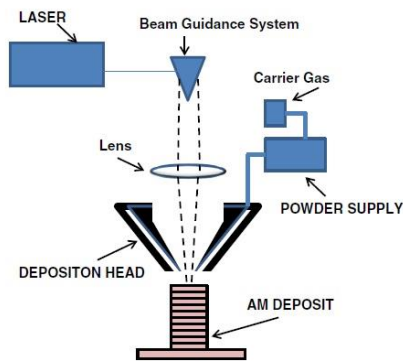


Figure 2.6: Representation of a powder nozzle feeding system [18]

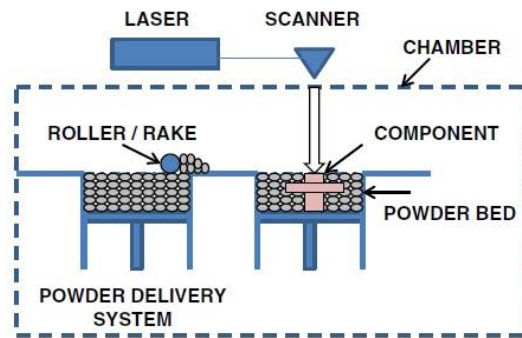


Figure 2.7: Representation of a powder bed feeding system [18]

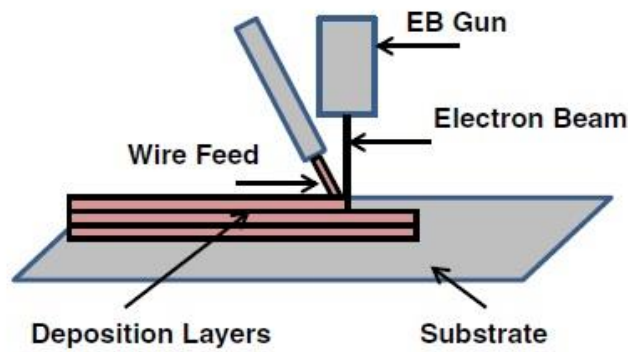


Figure 2.8: Representation of a wire feeding system [18]

The characteristics of the raw materials prior to use on those processes must be controlled and defined for each application, besides the chemical composition of the materials, the feeding rate, wire diameter or powder granulometry are crucial to the operation and final properties of the produced part.

2.1.1. Electron Beam Additive Manufacturing (EBAM)

Electron Beam equipment working principle is based on the accelerated motion of the electrons, originated by electric and magnetic fields, in order to create a focused beam of with high energy density, which may be used in many applications such as: welding , cutting and of course AM applications. The parameters to be controlled in this technology are:

- A vacuum atmosphere, to avoid the electron to collide with other atoms that are not the work piece/raw material;
- Acelerating voltage;
- Atomic number of the working material;
- Electron kinetic energy

Electron Beam Additive Manufacturing is a process that produces near-net-shape parts by using a focused electron beam in a vacuum environment to create a melt pool on a metallic substrate, very similar to the electron beam welding process [21]. The process is similar to Selective Laser Sintering (SLS) [22].The electron beam travels in a path according to the piece “slicing” in order to process the parts layer by layer (Figure 2.9), melting the metal powder bed or wire promoting a columnar crystal growth. The metal feeding mechanisms can be made by a powder bed or wire, with the particularity that the wire must be submerged on the melting pool [23] [24].

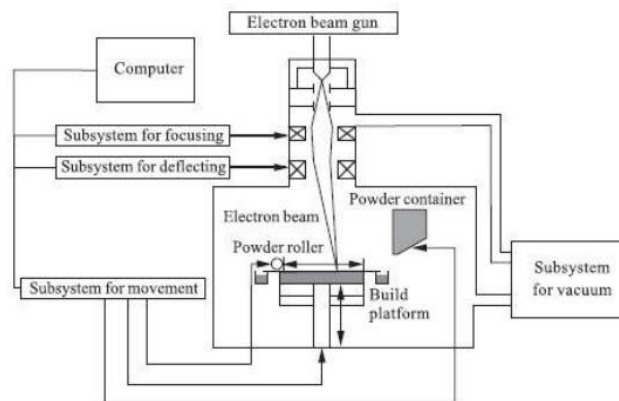


Figure 2.9:Representative scheme of the EBAM process [25]

Typically, EBAM characteristics are:

- High dimensional precision;
- Fast travelling speed but small deposition rate, which can be improved by using a wire feeding system, that is usually adopted in processes with the goal to increase deposition rate;
- The low pressure environment allows to avoid the heat loss by convection, which implies that the final metallurgical properties, such as porosity, are superior comparing to Laser Additive Manufacturing (LAM) [27];

- The powder removal from the part, in powder bed systems requires an additional operation[28];
- The parts size are limited due the process chamber size (Figure 2.10),
- High capital cost for equipment ;

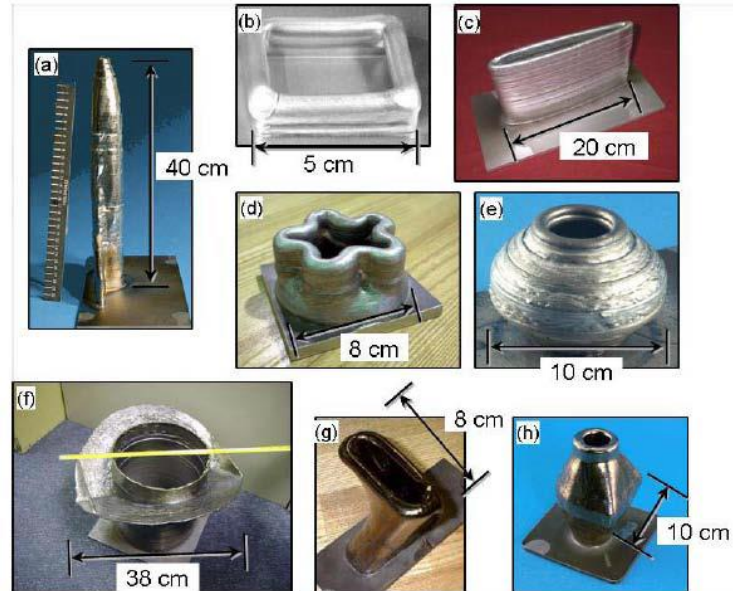


Figure 2.10:Parts manufactured by EBAM process [26]

2.1.2. Laser Additive Manufacturing (LAM)

Laser Additive Manufacturing (LAM), is a technique to produce parts, very similar to the EBAM technique that uses a laser power source instead of using an electron beam as a power source. The parameters of this process, are [29] [30]:

- Power;
- Processing speed;
- Feeding rate, powder or wire, if it is wire the diameter must be considered;
- Working atmosphere;
- Beam diameter;
- Distance between contact tip to the work piece;

There are several LAM processes but in this work only techniques the three most used: Selective Laser Sintering (SLS), Selective Laser Melting (SLM) and LENS (Laser Engineered Net Shaping) [31] (Figures 2.11, 2.12 and 2.13).

The main characteristics of LAM are:

- High dimensional precision, regarding the thickness of the walls;

- Fast processing speed and small deposition rate;
- Limited part size due the chamber space to operate, if the process occur in a closed chamber;
- In powder bed feeding systems, the Hot Isostatic Pressing (HIP) processing is used commonly in order to improve the mechanical characteristics of the part and increase the part density [27] [32];
- Low energy efficiency [33];
- High investment cost;
- The wire feeding system is very difficult to automate due the alignment concerning the laser beam and the wire [34] [35], but the component produced presents better properties;
- In powder bed systems, the absorptivity of the powder raw materials is generally too low, which requires more energy to operate [36].

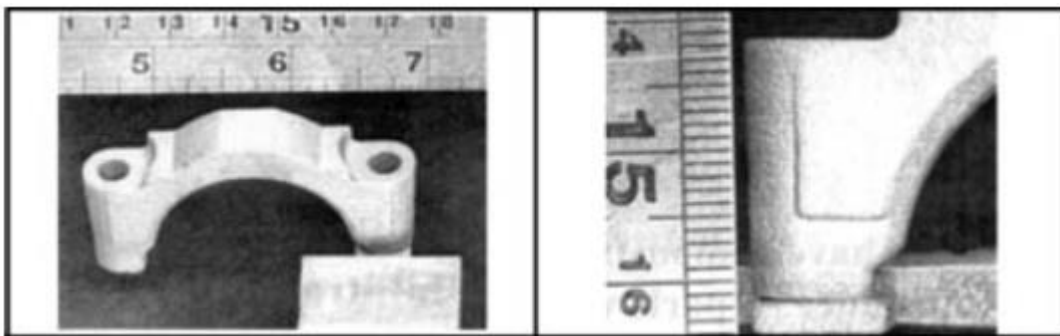


Figure 2.11:Aluminium functional part manufactured by SLS process [37]

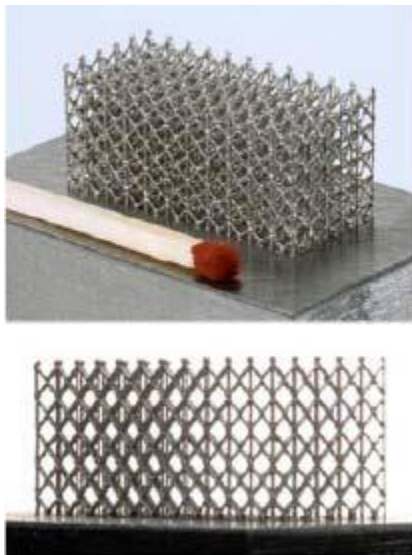


Figure 2.12: Metallic structure fabricated by SLM process [38]



Figure 2.13: Manufactured part and processing using LENS technology [39]

The SLS process can be described in two stages: the powder bed feeding by dragging the powder to the processing zone and secondly, the laser beam will process the layers of the cross section part in a repeatable operation. When using the powder bed feeding system, the metal powder is

preheated in order to facilitate the sintering phenomenon and an Argon atmosphere is used to process some reactive metal (e.g. Titanium) [25].

The main properties of this technique comprise:

- High dimensional precision, higher than EBAM;
- Fast processing and a small deposition rate;
- Typically , the SLS equipment uses a CO₂ laser;
- Low porosity, good mechanical properties on the final parts;
- Many parts can be built in the same processing system, which can reduce cost and improve productivity.

SLM is an AM process very similar to SLS, but instead of sintering the metal powder or partially melt it, the metal is totally melted under the Laser beam focused zone (Figure 2.14) [51]. This technology is more recent than SLS, and can be very promising since with the appropriate parameters it can process materials like carbides and tool steel maintaining their properties in bulk [25].

The characteristics of this process are almost the same comparing to SLS, except:

- Generally it is used to process metallic materials and metallic alloys, that are previous mixed to form the powder bed;
- The metallurgical aspects of the finished part need to be strictly controlled due the heat loss from the part and the cooling rate [40].

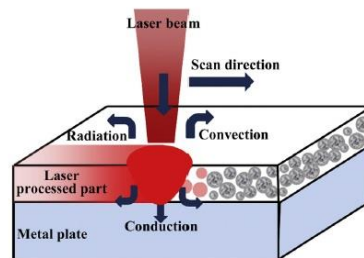


Figure 2.14: Representative scheme of the SLM/SLS process [9]

Laser Engineering Net Shaping is an AM technique that processes a solid part by depositing metal powder on a melt pool created by a laser beam [41]. The working part of the LENS consists on a laser beam and a nozzle that feeds powder directly to the operation zone. The process takes place in an atmospherically controlled environment usually of argon gas [42] (Figure 2.15).

The first step of the operation is to focus the laser beam on a metal part to create a melt pool. Next, the metallic powder is delivered from the nozzles to add more volume, repeatedly in order to build a layer upon layer until the complete part is built.

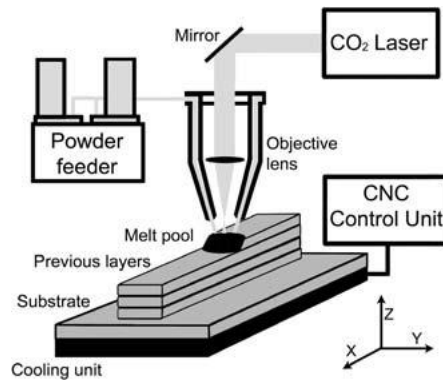


Figure 2.15: Representative scheme of the LENS process [44]

The main characteristic of this process include:

- The powder is fed on a hopper, in an independent system different from SLS and SLM that use a powder bed feeding system;
- This technology is focused to process a large variety of metals;
- The final part has a good dimensional accuracy, though not as good as EBAM, and leads to solid, fully dense characteristics, similar to traditional processes [42].

2.1.3. Wire and Arc Additive Manufacturing (WAAM)

Wire and Arc Additive Manufacturing are processes that use some technologies as in arc welding but differ from LAM and EBAM since the equipments used are the same as for welding. These technologies are receiving considerable attention due to the capability of producing large complex parts, in large productions at lower cost, in comparison with EBAM and LAM Processes [45].

WAAM were introduced by Baker when vessels and containers were manufactured by overlapping layers of metal using the Shielded Metal Arc Welding (SMAW) process [46]. Almost 100 years later, WAAM is a competitor of the other Metal Additive Manufacturing processes developed nowadays though arc welding technology for manufacturing has been used in the 70's by the largest steel making company in Germany, *Thyssen Hütten AG*, using the Submerged Arc Welding process [7]. Plasma Arc Welding (PAW) [47], Gas Tungsten Arc Welding (GTAW) [42] [48]; Gas Metal Arc Welding [49] [50] are the processes studied nowadays for AM that present very specific features such as:

- Welding Current (I) , Traverse Speed (TS) and Wire Feeding Rate (WFR) are the main parameters but there are others to consider, depending on the process;

- These processes have in common, the energy source and, the wire feed system with the exception the PAW process which also uses the powder feeding system, [42];
- The mechanical and metallurgical properties can be controlled by the selection of parameters. A large diversity of metallic materials can be used for production, obtaining solid fully dense parts [42];
- The processes can be automated;
- The energy efficiency is better than EBAM and LAM [45];
- WAAM techniques are not limited by the parts dimensions like LAM and EBAM (Figures 2.16 and 2.17);

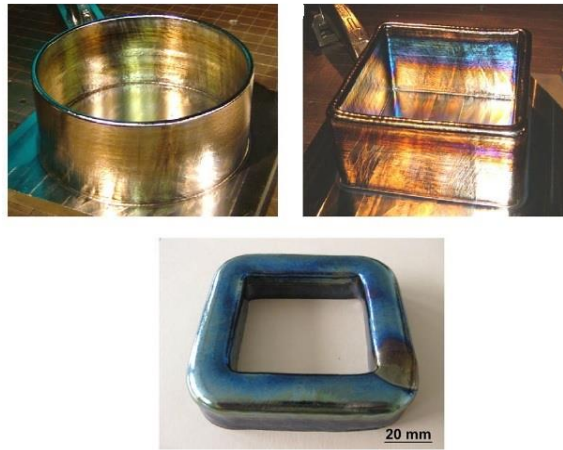


Figure 2.16: Tubular Ti-6Al-4V components made by WAAM processes [42]



Figure 2.17: WAAM manufactured part before machining (left) and after machining (right) [39]

GTAW (Figure 2.18) is commonly used and known as a welding process which is adopted by industries that need high quality welding. The arc is established between non consumable tungsten electrode and the part in an inert gas shielding atmosphere [51].

The advantages of using this process in AM are:

- Free slag and spatter process;

- The wire can be preheated in order to facilitate its fusion, generated by an independent system providing the energy by Joule effect [51];
- Good morphology of the deposits and reasonable dimensional accuracy, comparing to LAM and EBAM;
- Dense metallic parts and well known metallurgical properties of the final part

Plasma Arc Welding (Figure 2.19) is very similar to the Gas Tungsten Arc Welding process, since in both processes it is used a non-consumable tungsten electrode. The plasma formation and the energy density are the key factors that differ from GTAW. In the plasma welding, the plasma is due to the constriction in the nozzle and the high electrical density [51].

The most important features are [52]:

- The use of two gas systems, shielding gas (Argon, Helium or mixtures with Nitrogen and Hydrogen) and plasma gas (only inert gases like Argon or Helium);
- Working current can be DC or AC, but typically DC+ current with non-transferred arc is used [17];
- High power density, which means that the productivity can be higher than other WAAM technique;

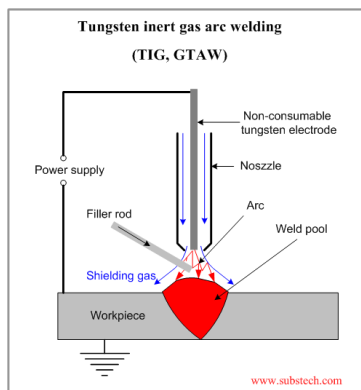


Figure 2.18: Representative scheme of the GTAW process [54]

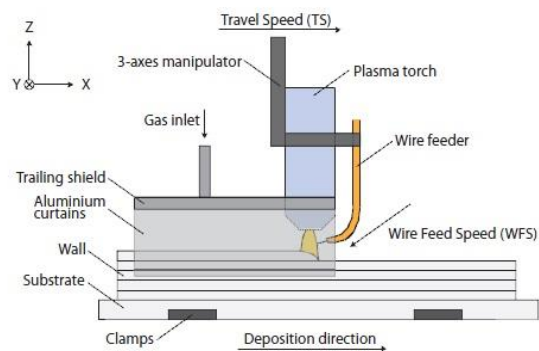


Figure 2.19: Representative scheme of the Plasma Additive Manufacturing [47]

GMAW is a welding process that uses a consumable wire with small diameter, allowing having a high melting rate.

Gas Metal Arc Additive Manufacturing (GMAAM) technologies can be automated in order to produce 3D parts by overlapping layers of metal by deposition in the same conditions as GMAW. The process parameters will influence, among other aspects, the metal transfer mode which in turn influences the result obtained. The existing transfer modes in GMAW are:

- Short circuit transfer, which occurs when the wire electrode melts in the melt pool and is identified by high Voltage, low current intensity and low feeding rate;
- In globular transfer, the metal deposition is essentially due to gravity, and the parameters are low voltage and feeding rate, and medium current intensity;
- Spray transfer, is used to obtain high mass transfer of material and the parameters required are high feeding rate, Voltage and current intensity.

These transfer modes leads to different morphologies and metal rate depositions and opens possibilities to use the GMAW variants in order to adjust the metal deposition for the results required.

In GMAW (Figure 2.20), the most used variant for AM is the CMT (Cold Metal Transfer). CMT is based in a controlled dip transfer mechanism and the main advantage is the lower thermal heat input [7]. The process occurs when the wire dives in the molten pool after which there is a voltage drop, followed by a short circuiting of the current. This phenomenon occurs repeatedly during the operation (Figure 2.21). The low thermal heat input is an advantage associated with excellent finishing quality and spatter-free metal deposits [53].

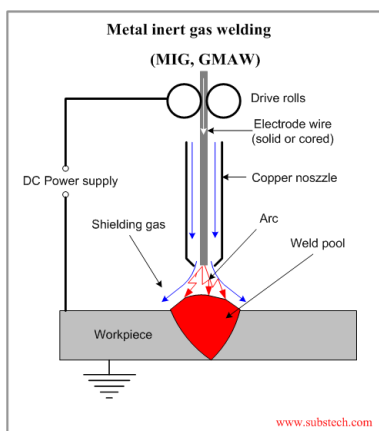


Figure 2.20: Representative scheme of GMAW [54]

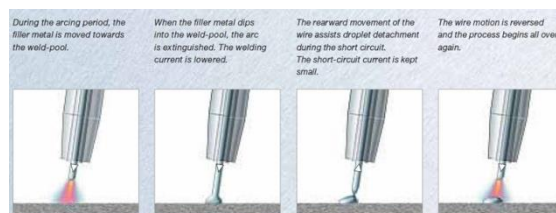


Figure 2.21: Representative scheme of the CMT operation cycle [55]

In summary, the main properties of EBAM, LAM and WAAM processes can be presented on a comparative table. Table 2.1 compares those techniques in a relative quality assessment in Low, High and Very High, for several parameters:

	EBAM	LAM	WAAM
Part finish	Very High	High	Low
Deposition Rate	Low	Low	High
Acquisition Cost	Very high	High	Low
Energy Density	Very High	High	Low
Part size range	Low	Low	Very high

Table 2.1:analysis of different additive manufacturing processes

2.2. Metal Additive Manufacturing Summary

From the analysis of different technique used for AM, the following can be concluded:

- AM is a promising manufacturing process for metals because it can produce metallic complex parts, is adaptable to different designs quickly without increasing costs, eliminates the need of vast inventories, leads to reduction of the waste rate combined with energy saving in the entire process, in comparison with other traditional manufacturing processes;
- The AM technologies explored on this work have many advantages comparing with traditional manufacturing processes, but the final part requirement for use have a critical role in the decision for the adoption of a given AM technique;
- WAAM is interesting to explore, mainly for light alloys, because WAAM presents a higher productivity than LAM and EBAM. WAAM working principles are well known for many years because they are used commonly on welding applications. This method has been studied and used by some companies on a diversity of AM applications in metallic alloys such as Titanium, Nickel, Stainless and Tool Steels and Aluminium, as shown on the Table 2.2, the studied metallic materials in AM processing, regarding the scientific publications.

Materials used	Publications
Titanium alloys	[21, 24, 28, 29, 42, 48, 57, 58, 59, 60, 69, 71, 75, 77, 79, 80, 81, 82, 83, 84]
Nickel alloys	[24, 60, 66, 76, 78, 83, 85]
Tool steel	[41, 63, 72, 89, 90]
Stainless Steel	[61, 64, 65, 70, 73, 74, 80, 87, 88]
Aluminium	[40, 62, 67, 68, 93, 94, 95]
Copper	[95, 96]
Cobalt	[91, 92]

Table 2.2: Publications made on AM regarding only the materials used

2.3. Aluminium

2.3.1. Properties and Applications

Aluminium is widely used on a diversity of applications due to its intrinsic properties specially its density, $2,68\text{g/cm}^3$, which is important in the most of the applications with an excellent mass/volume ratio associated to its mechanical properties, becoming a good option for several industries like automotive and aerospace. Aluminium also is known by the excellent thermal and electrical conductivity allowing the use of aluminium alloys in electrical cables, for example. It is known that aluminium and its alloys are ductile which allows to deform easily, and combined with its corrosion resistance can be a choice for packaging ends.

In summary, the aluminium can be characterized by:

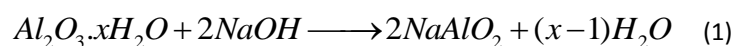
- Ductility;
- Low density;
- High thermal and electrical conductivity;
- Corrosion resistance and the several types of surface treatments and coating applied on these alloys;
- Recyclability.

2.3.2. Production

Nowadays the aluminium production is divided in two parts: primary and secondary.

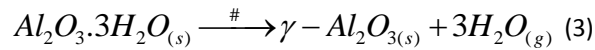
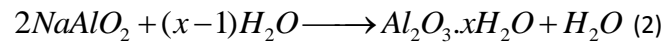
In the primary aluminium production process the beginning of the process is the extraction of the aluminium which may be made by two processes: the Bayer process and the Hall-Héroult process.

The Bayer Process is used to refine the alumina and consists in the dissolution of the bauxite in a high concentration aqueous solution of Sodium hydroxide at approximately 240°C . Most of the alumina is dissolved, remaining what is called “red mud”, a residue that contains mainly Iron and Silicon oxides. The parameters to control in this process are the pressure and the Sodium hydroxide concentration that is adjusted in order to the bauxite nature; this process step can be summarized in the following equation [97].

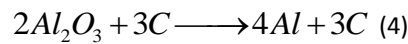


In the second stage of the Bayer process, the reaction is inverted in order to obtain just the alumina, and it is accomplished by the cooling of the reaction product in order to precipitate the trihydrated alumina crystals in the solution. This operation occurs in a temperature approximately about 50°C and the receptacles have very low agitation. The trihydrated alumina is removed and washed with sodium hydroxide, in order to reuse once that is not consumable in the process and after this the

trihydrated alumina is calcinated at temperatures between 400°C and 600°C, and forms γ -alumina instead of α -alumina because it is chemically active. The reactions that represents this stage are [97]:



The Hall-Héroult process consists on dissociating de aluminium from alumina using an electrolytic reduction cell. Since alumina has a melting point of 2400°C and a poor thermal conductivity, the key to extract aluminium from alumina is to insert the Alumina in a high concentration cryolite bath, in a proportion of 80%-90% of cryolite for 2%-8% of Alumina, with additives like CaF_3 and AlF_3 . The reduction cell consists on consumable baked carbon anodes and promotes the reduction of the aqueous solution, described by the following equation [97]:



The secondary production of aluminium it is based on recycling the aluminium alloys residues and produces less solid residues and energy spending, as can be observed in the following figure (Figure 2.22).

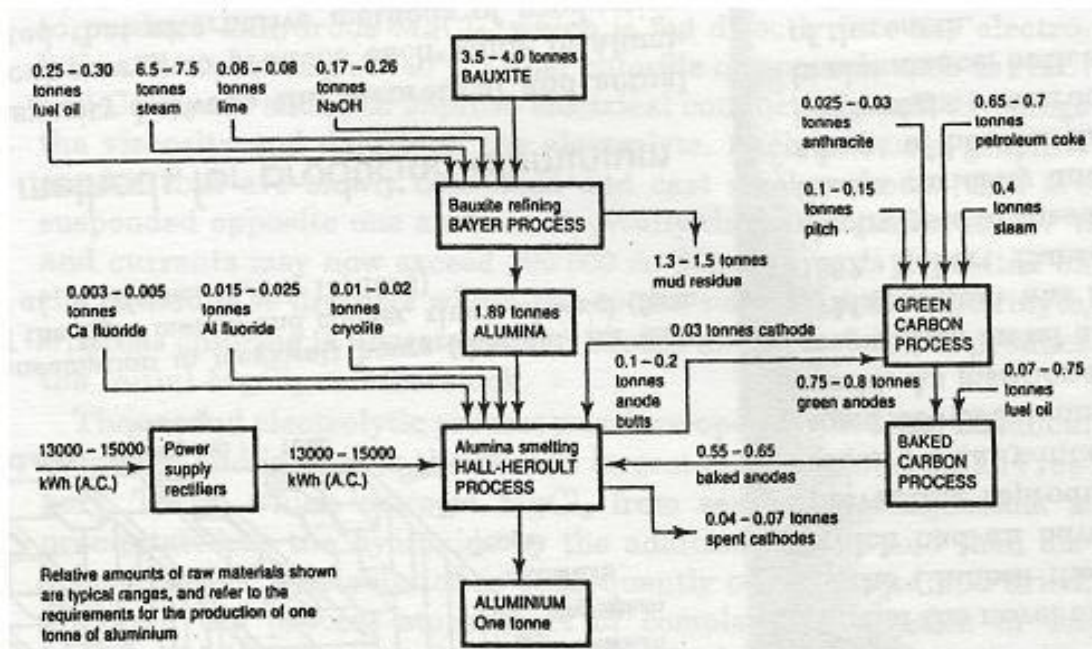


Figure 2.22: Aluminium elaboration process [98]

2.3.3. Alloy designation and treatments

Aluminium alloys selected for mechanical behavior are classified according with the most predominant alloy element. The designation used consists on a combination of four numbers to identify the Aluminium alloy, the first two numbers show which elements the alloy have in its composition and the remaining two numbers reveal the modifications or the impurity limit on the original alloy.

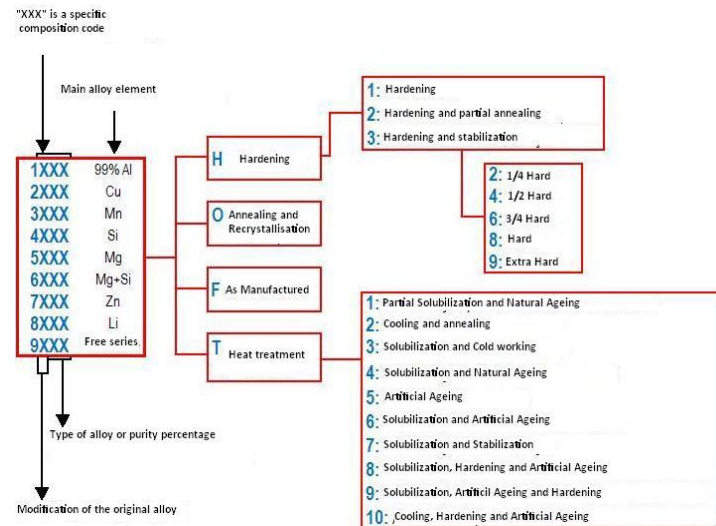


Figure 2.23: Aluminium alloy series and its heat and mechanical treatments [98]

In the figure above (Figure 2.23) the schematic representation of the several alloys. Heat and mechanical treatments are represented but there is a division between the alloys thermally treated (2xxx, 6xxx and 7xxx series) and the alloys non thermally treated (1xxx, 3xxx, 4xxx and 5xxx series).

2.4. Gas Metal Arc Welding

The GMAW welding process is an arc welding process that uses an electric arc between a consumable metallic wire, which is fed through a copper contact tube which conducts the welding current into the wire. The wire is fed directly in the weld pool. This process use shielding gas that is supplied from an external source. The shielding gas is chosen according to the application required, either inert gas (MIG) or active gas (MAG) (Figure 2.20), being the shielding atmosphere crucial because affects the process parametrization and the metallurgical/mechanical properties of the deposited metal [51].

Usually it operates with the DC (+) and with a wire diameter (usually between 0.6 and 1.6mm) and wire feed speed determine the welding current, as the burn-off rate of the wire will form an equilibrium with the feed speed.

The parameters to adjust in this process are:

- Current (I);
- Voltage(V);
- Wire Feeding Speed (WFS);
- Travel Speed (TS);
- Polarity;
- Welding position;
- Atmosphere.

This welding process has advantages compared with other welding processes, such as:

- Commercially available metals and alloys can be welded by this process,
- High productivity process in terms of deposition rate and can be used either manual or automated;
- This process can be used in all welding positions;
- Higher travel speeds can be achieved than other electric arc welding processes;
- The slag formation is minimal due to the shielding gas usage;

GMAW has four typical transfer modes which are short-circuiting, pulsed arc, globular and spray.

2.4.1. Short-circuiting transfer

Short circuiting transfer, as known also as dip transfer, in GMAW is characterized by low arc current, voltage and certainly a low heat input, which is useful to weld parts with low thicknesses. Due to its characteristics, the weld pool solidifies at very fast rates. The metal is transferred from the electrode to the work piece only during the time the electrode contacts with the weld pool, the complete cycle of short circuiting transfer is represented in Figure 2.24.

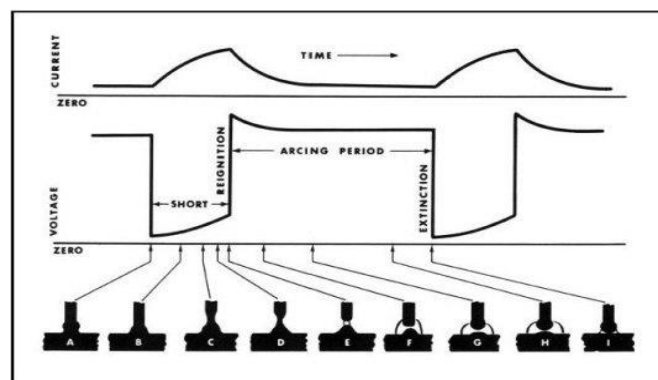


Figure 2.24: Cycle duty of short circuiting transfer [52]

Short circuit metal transfer can be described in three stages. The first phase is located between the points A and D (Figure 2.24) and corresponds to an increase in welding current and voltage and when the molten tip of the wire is dipped to the welding pool guaranteeing the quick transfer of the molten metal. The second phase occurs on point E, the voltage is increased instantly and the electrode is separated from the weld pool. Finally, the third and last phase denoted by arcing period, occurs between point E and I, after the tip of the electrode separates from the weld pool, begins the melting of the electrode type, meaning the beginning of the new cycle. In this phase, the current must be as low as possible in order to avoid spatter formation [100].

2.4.2. Pulsed Arc Transfer

Pulsed transfer was introduced in order to improve spray transfer by lowering the medium currents, facilitate the transition to spray transfer mode. The electric arc is maintained by a low intensity current, and instantly the current suffers a high increase and promotes the metal transfer, as shown at the figure above (Figure 2.25):

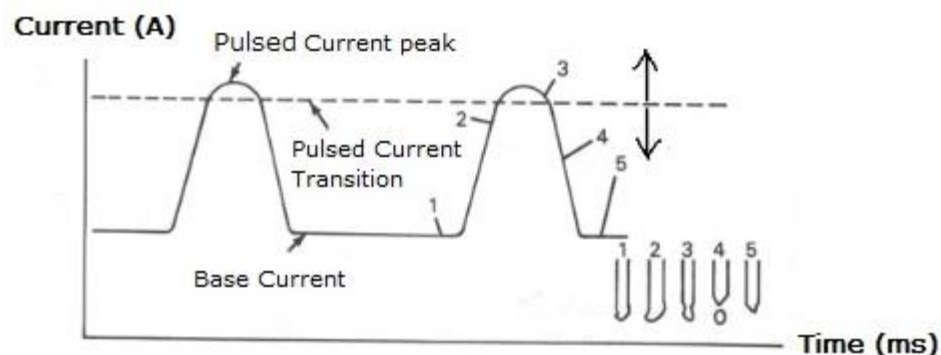


Figure 2.25: Pulsed transfer mechanism representing Current vs. Time [99]

For this transfer mode, the high current pulses can be obtained from a single phase rectifier connected to a rectifier power source as used for short circuit transfer. The main advantages for this transfer mode are the lower heat input due to the intermittent current pulses, and the higher deposition because the droplet detachment is similar to spray transfer.

2.4.3. Globular Transfer

Globular transfer is the less desirable transfer mode in MIG/MAG welding because that the heat input is too high, the welds surface and morphology is poor, generates a high quantity of spatter and works at the low speeds. It can be concluded that is the less productive welding process. This transfer mode is known by the drop size diameter higher than the electrode diameter and transfer occurs with

relatively low current, where the drop is transferred mainly by gravity force. The typical parameters to operate in this type of transfer are: medium voltages, medium currents and low feeding rates.

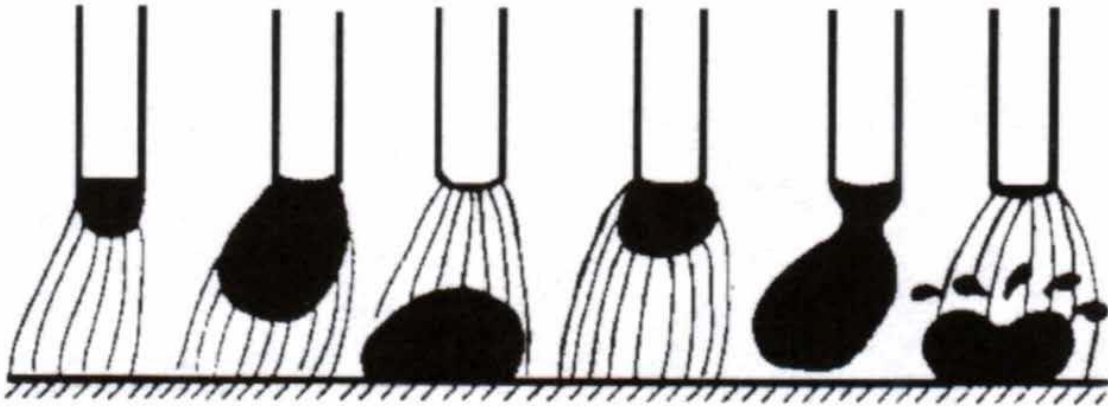


Figure 2.26: Globular transfer scheme in GMAW process [52]

2.4.4. Spray Transfer

Spray transfer mode is used to transfer high mass material, which means that this mode presents a higher deposition rate than the others. When the current is above the transition value, this type of metal transfer is characterized by small droplets transferred between the electrode and the work piece. The droplets are transferred at a rate of hundreds by second and are accelerated by electromagnetic forces. This type of metal transfer mode can achieve deeper penetrations than other transfer modes and also higher melting rates. The spray transfer is not used to weld thin sheets or to make root passes because the heat input is too high, so it used mainly as a filling process. The necessary parameter conditions to initiate the spray transfer are high voltage, current and feeding rate.

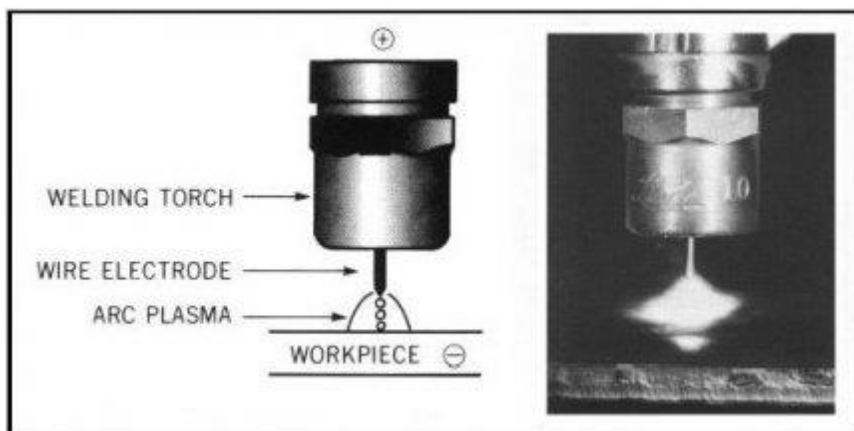


Figure 2.27:GMAW Spray transfer schematic [101]

2.4.5. Cold Metal Transfer (CMT)

GMAW processes adapt through time in order to improve the productivity of the process and the quality of the weld itself. In order to achieve that directive, *Fronius* introduced a new variation of the GMAW process called CMT. CMT is characterized by low heat input compared to the conventional GMAW, producing free spatter welds combined with low dilution of the base material [102]. The CMT operation mode consists in four steps (Figure 2.28 and 2.29):

- Step one: The wire move towards the workpiece and the arc is formed (A), due to the increase of the voltage. The significant current increase as well;
- Step two: The droplet is formed and the wire reverses its motion associated with the arc extinction (B). In this phase the weld pool is formed;
- Step three: The wire retracts, detaching the droplet in to the workpiece (C). The voltage drops to values near zero;
- Step four: This is the stage and the beginning of a new operation cycle: the wire motion reverses again and the arc is reignited (D).

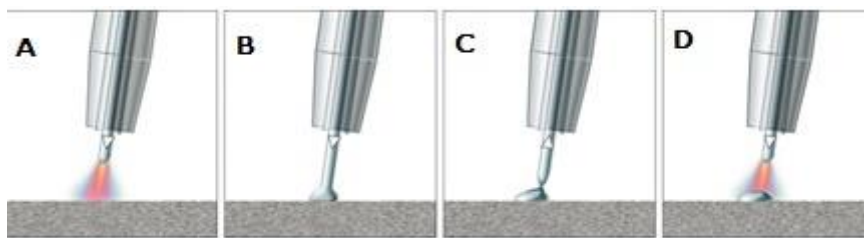


Figure 2.28: CMT operation cycle

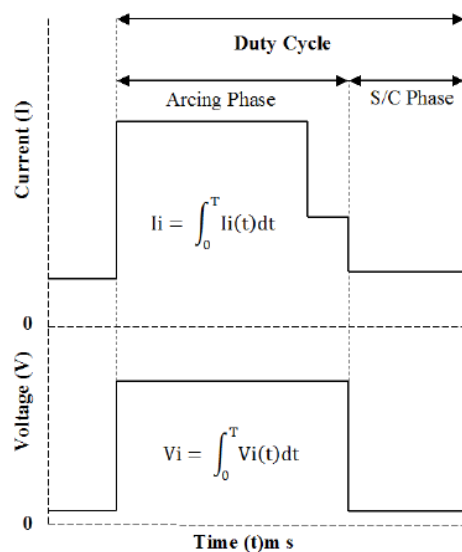


Figure 2.29: Current and voltage variation through time in a single CMT operation cycle [102]

This capability in the operation is determined by the motion of the electrode directly assisted by the process control of the parameters chosen. This forward and backward motion takes place at a frequency of up to 70 Hz. CMT can be applied to weld the most of the materials with low heat input, meaning that the thickness of parts is not a barrier to use this process and also to fuse some high melting point metals and alloys. Its productivity compared with GMAW is higher considering that the deposition rate can be higher and the possibility to operate at higher travel speeds (TS), becoming an excellent arc welding process for AM applications.

2.5. Literature review summary

Additive manufacturing reveals itself as an innovative manufacturing technique, offering solutions to complex parts produced in low batches. Nowadays, the main interest developed in the industry is the metallic part fabrication in order to offer effective low cost solutions.

Metal additive manufacturing techniques were mainly developed from the welding technologies, mainly electron beam and laser welding, and in order to improve the productivity of the AM technique in terms of deposition rate, the electric arc processes started to be studied.

In order to improve the MAM, the electric arc processes were used for this technique and this work takes a focus in the quality of the parts, taking in account that the non destructive tests can be studied as well, corroborated by destructive tests, in order to offer a simple, cost effective and reliable solutions for MAM.

3. Experimental Procedure

In this chapter the experimental work is described, considering all the stages including materials, equipment, preparations and procedures for the work.

3.1. Layer by layer wall building

In order to study AM with CMT arc welding process it was necessary to define what geometry should be adopted in order to facilitate the study of the properties along the wall section. The available equipment allowed building linear walls, which in this research work was the desirable geometry in order to ease all operations as it will be shown later on this work. In this stage, the electrical welding parameters were acquired and analysed with a data acquisition (DAQ) system in order to determine the real medium voltages and currents used in the process.

The equipment and materials used for this task were:

- *Kuka* 6-axis robot system;
- *Fronius* CMT welding equipment + parameter controller;
- Welding wire consumable ESAB ER5356, composition almost similar to Aluminium alloy AA5083 (Appendix A) and a diameter of 1mm;
- Substrate plates of Aluminium alloy 5083 with the dimensions of 300mm x 50 mm x 15mm;
- Clamping system;
- Argon shielding gas 99,9% atmosphere;
- National Instruments DAQ software + device;
- Voltage and current transducer;



Figure 3.1: Kuka 6-axis robot



Figure 3.2: Fronius CMT VR 7000



Figure 3.3: Fronius parameter controller RCU 5000i



Figure 3.4: National Instruments DAQ device



Figure 3.5: Current transducer LEM LT 500-S



Figure 3.6: Tension transducer LEM CV 3-200/SP6

The trajectory defined for the robot to operate with the welding equipment was a linear trajectory in order to produce straight walls, so the first trajectory defined was a linear one way trajectory.

The first iterations to build walls were not successful due to the fact that the robot kinetics was not considered, so the aspect of the first deposits is shown in Figure 3.7.

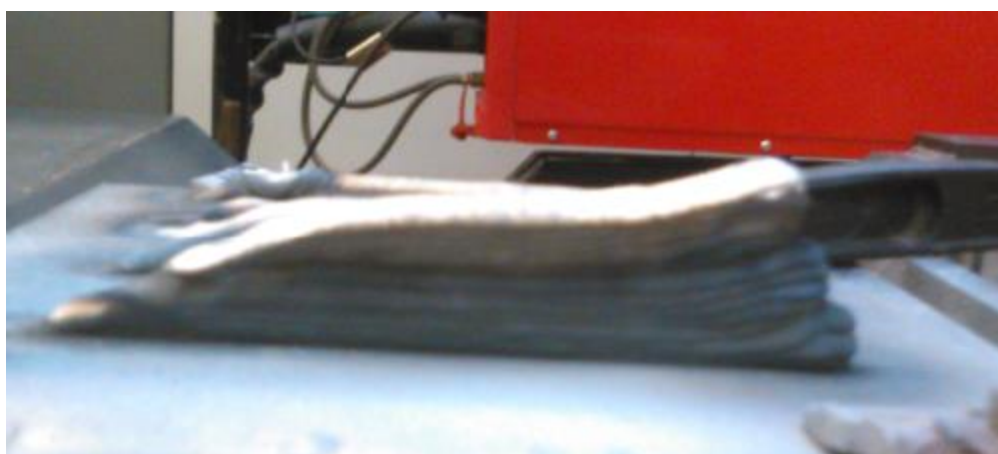


Figure 3.7: Wall build up first iteration

In order to solve this problem, the trajectory changed and the new trajectory adopted was a two way trajectory in the same direction. With the same welding parameters the results were successful and the built walls were viable to study afterwards (Figure 3.8).

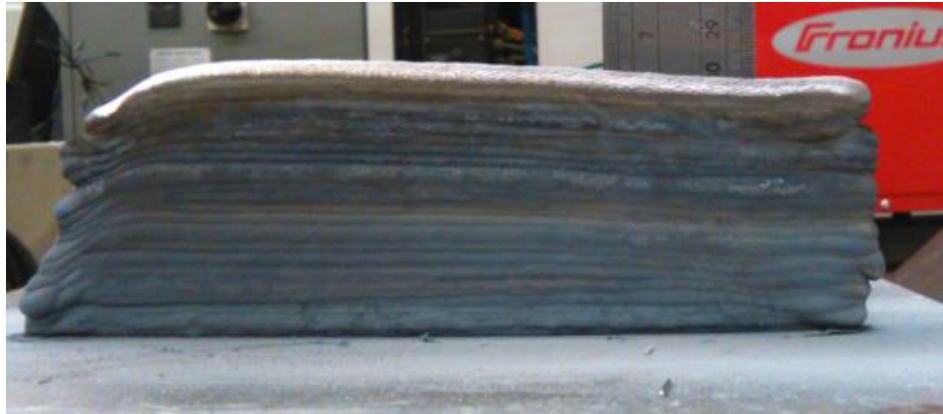


Figure 3.8: Wall build up second iteration

The next step in wall building task was to adjust the welding parameters and the wall dimensions.

Primarily, the welding parameters were chosen according with the preliminary tests done previously and the objective was to study the variation according the Welding current, so the Current range chosen was between 130A and 60A, skipping 10A at each wall. In CMT parameter control, Voltage and Current are controlled according to the imposed Wire Feeding Rate, so the remaining parameters were fixed, as shown in Table 3.1.

Current (A)	Voltage (V)	Wire Feeding Rate(m/min)	Travel speed (mm/min)	Gas Flow rate (L/min)	Torch Angle (degrees)	Stick-out length (mm)
130	17.6	11.4	600	17	0	15 -- 20
120	17.3	10.4	600	17	0	15 – 20
110	16.9	9.3	600	17	0	15 – 20
100	16.5	8.5	600	17	0	15 – 20
90	16	7.6	600	17	0	15 – 20
80	15.6	6.8	600	17	0	15 – 20
70	14.9	6.0	600	17	0	15 – 20
60	14.1	5.2	600	17	0	15 – 20

Table 3.1: Initial parameter setting defined for wall buildings

After deciding the robot trajectory and the parameters on the welding equipment to use in order to produce good quality walls, the next steps to prepare were:

- Decide what wall dimensions, in particular about length and height in order to prepare the substrate plates;
- Connect the DAQ system to current and Voltage transducers to determine the real voltages and currents.

The wall dimensions were planned according to the substrate plate dimensions and so that there was enough material to analyse afterwards and for some consequent machining. The dimensions chosen in length and height, taking in account the previous considerations, were respectively 250mm and 30mm.

3.2. Current and Voltage Data Acquisition

During the wall build up the current and voltage data were acquired to determine the Heat Input in the process properly and also for the determination of the Process Efficiency.

The *Fronius* Controller RCU 5000i shows average values for each parameter, so in order to assure that the real parameters were measured, independent equipment was used to measure each one of the parameters. The parameters that vary in CMT welding, are Current, Voltage and Wire feeding rate, so the calibrations were made for each one of the parameters starting with the Wire feeding rate (WFR).

In order to determine the real WFR, the following methodology was applied:

- Introduce a value of WFR on the controller;
- Turn on the wire feeding instruction of the welding equipment to feed wire,
- Turn off the instruction after ten seconds and measure, in meters, the wire length fed during this time interval;
- Multiply that measurement per six and obtain the real value of the WFR in meters per minute.

The values obtained were equal to the display in the controller so this parameter does not need much more adjustments.

The other two parameters were not that simple to determine and for that purpose the material needed for this task was:

- Current and Voltage Transducer;
- DAQ system device and software *National Instruments LabView Signal Express*;
- 9V battery.

Using the *National Instruments LabView Signal Express* DAQ software, the calibrations were made by a simple welding test for current data to compare with the manufacturer current range. To

ensure the Voltage values for de DAQ, the 9V battery was simply plugged on and the measuring was made directly from the Signal Express software. Both equipment values acquired were validated with success.

3.3. Deposition Efficiency and Heat Input calculation

In this task the Process Efficiency and Heat Input were calculated and in this process the two ratios are directly dependent from each other. The process efficiency it is a ratio between the material deposited on the substrate plate and the welding wire fed for the process.

The steps followed to determine the process efficiency were:

- Before the wall manufacturing, the substrate plates were all weighed;
- Build the walls;
- Remove the plates with the walls and weigh again;

After acquiring the data, this was treated in order to calculate the process efficiency and Heat Input by using the following equations:

- Weight of electrode used (WEU):

$$WEU(g) = WFS \cdot A_e \cdot \rho \cdot t_w \quad (5)$$

- Deposition Efficiency (DE):

$$DE(\%) = \frac{mass_{before} - mass_{after}}{mass_{electrode}} \times 100 \quad (6)$$

- Heat Input (HI):

$$HI(kJ / mm) = \frac{V \times I \times 60}{WS \times 1000} \times \eta_{MIG} \quad (7)$$

The efficiency of the MIG welding process is considered 0.8 [102].

3.4. Non Destructive Testing

Nowadays, Additive Manufacturing (AM) technologies are growing in the market and the industries are more willing to adopt AM techniques. The study of AM parts is developed, however quality control of AM parts has not been widely studied with non destructive testing techniques.

There are several NDT techniques: Visual Inspection (VI), Liquid Penetrant Testing (LPT), Magnetic-Particle Testing (MPT), Radiation Testing (RT) using X-Rays or γ -Radiation, Eddy current testing (ECT) and Ultrasonic testing (UT). VI, MPT and LPT are mainly used to identify surface defects on the parts and Radiation and UT for surface and bulk defects.

In this work the UT technique will be tested in AM parts in order to evaluate reliability of this technique using pulsed echo and phased array, due to their advantages (Table 3.2).

In pulsed echo mode, the sound is emitted by the probe and the measurements are made by the travelled sound wave, emitted and received by the probe (Figure 3.9). The travel time is measured and the wave speed is known, due to these facts the calculation for the wave travel distance is simple. The representation for the results of this test is the A-Scan [103].

In phased array ultrasonic testing, the probe emits a spherical (or cylindrical wave) with a relative delay in time, and according the Huygens Principle, the set of elementary waves, build an angular wave front of focus point (or line) [104]. This is the concept that defines the phased array phenomenon (Figure 3.10).

UT presents the following advantages and limitations:

ULTRASOUND NON DESTRUCTIVE TEST	
ADVANTAGES	LIMITATIONS
<ul style="list-style-type: none"> • High penetration power • High sensitivity • Accuracy on the determination of the position of the reflector • Only requires access on the one side • Instant response • Capability for automation • Inspect the entire volume of the inspection part • No risk for people and operators • Portable equipment 	<ul style="list-style-type: none"> • Requires experienced operators • Requires extensive knowledge of experimental techniques • Difficult to apply on rough pieces of little thickness or irregular, because of the reflectivity of the materials • Difficult to detect near-surface discontinuities • Requires coupling means • Requires reference blocks, for equipment calibration

Table 3.2: Advantages and limitations of UT

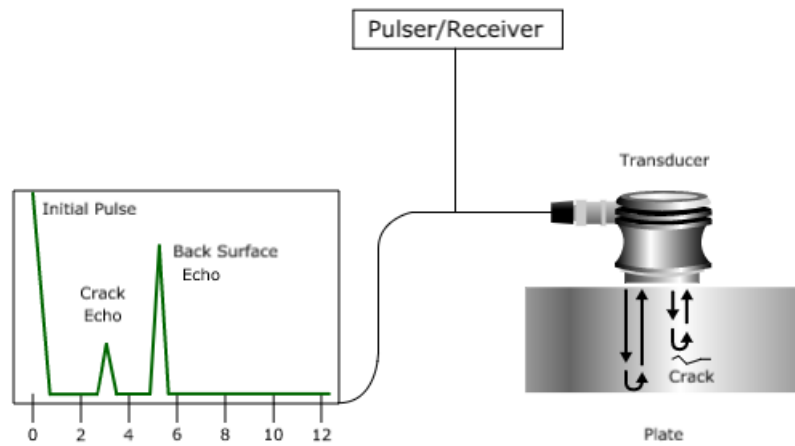


Figure 3.9: travelling process and signal acquisition regarding the existence of defects [103]

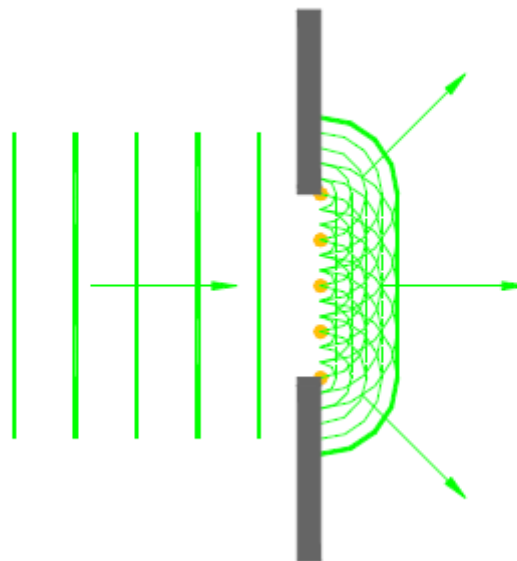


Figure 3.10: Huygens principle represented in the Phased Array UT [104].

The X-ray technique was also used for confirmation of the results obtained. The NDT radiation consists on the absorption of radiation that is differentiated in the test part and due to the composition, density and thickness of the parts, the amount of radiation absorbed varies along the part. The X-ray is a reliable test for parts in volume inspection.

Destructive tests and X-ray testing were performed in order to compare the results and achieve conclusions about the possibility of implementation of the UT pulsed echo testing for AM.

Equipment used for NDT:

- Transmitting and receiving probes;
- Conventional UT equipment GE USM 35;
- Coupling gel;
- Container with an aqueous solution and automated system for moving the probe;
- Data software used in PAUT: Multi 2000;
- Radiation source and film.

A difficulty that AM presents for UT is the coupling of the probe since the surface of an AM part, particularly those which are produced by arc welding, are rough. To avoid this problem, the back of the plate was used for coupling with the UT probe (Figure 3.11). The first approach, was the pulsed echo technique, which included the following steps:

- The plate was covered in a conductive gel layer in order to establish the coupling between the plate and the transmitting probe;
- The UT wave is emitted by the transmitted probe and received by the same probe, considering the plate thickness (6,5mm), and this process was done manually;
- The mechanical signal is transformed into an electrical signal, which is represented on a screen, with appropriate software just for analyzing the data presented in the A-scan, which represents the distance travelled by the wave and the intensity of the signal.

The second approach has the same mechanism but the plate was submerged into water and the part was fully scanned (Figure 3.12). The test is still an UT, but the sound waves used in this test were not the longitudinal waves as in pulsed echo technique but instead is used the Phased Array Ultrasound Technique (PAUT), as the name suggests an array of longitudinal waves are emitted by a matrix of small transducers, unlike the conventional manual A-scan probe with only one transducer. These small transducers are computer controlled and can be pulsed independently in a set sequence or phase; the pulses of sound interfering with each other to produce a sound beam of a certain angle. So, the following procedure adopted:

- Submerge the plate in water;
- Define the dimensions for scanning the part;
- Scan the part and collect the results.

The results collected show the travel distance made by the emitted and reflected wave, and if the peaks appear before the total thickness of the part, there is an interface that reflects the echo back to the probe, and thus a defect.



Figure 3.11: Surface of the plate used for the analysis, for both procedures



Figure 3.12: Experimental procedure equipment for the Phased Array test, where the plate is submerged and the scanning probe is coupled with the automated system.

The full part scan followed the trajectory described in Figure 3.13:



Figure 3.13: Trajectory made by the sound probe in the Phased Array ultrasonic testing

After the PAUT were performed, the sample was destroyed in order to validate the existence of defects, especially their locations and dimensions. After that, new parts were tested again by UT pulsed

echo test, with the same procedure acquiring the A-scan data, and this was followed by the Radiation testing for confirmation.

For the Radiation testing the procedure consisted in:

- Set the parameters needed for the test, voltage, current and time of exposure;
- Adjust the test part and the X-Ray tube, in order to guarantee a successful radiation absorption concerning the defects orientation.



Figure 3.14: Experimental setup for the radiation NDT

The NDT was performed in different materials, in one of the test parts of this work and one test part manufactured in the Cranfield University, made from carbon steel.

3.5. Macrostructure and microstructure analysis

In this work, after the NDT, the destructive tests were conducted in order to confirm the NDT results and evaluate other relevant characteristics.

Macro and micro analysis imply destroying the AM walls to produce samples from the welded sections. These tests allow observing defects like poor fusion, porosity, inclusions and other metallurgical aspects like grain size and precipitates.

Both tasks required the same four steps which were:

- Cutting samples from the AM wall: the samples were cut of the AM wall in order to inspect the wall section;

- Mount the samples in resin: samples were assembled in epoxy resin because generally the aluminium alloys suffer phase transformations at relatively low temperatures, so hot mounting is excluded,
- Grinding and polishing: for metallographic analysis the exposure of the surface is crucial, so the grinding and polishing operations were made in the same equipment using the mesh sizes: 600, 800, 1200, 2400 for grinding and polishing for 3µm and 1µm following the procedure described on Appendix B1;
- Etching: this operation consists on dipping the sample surface in chemical solutions for an interval of time in order to reveal the microstructure. In this work the solution used was the Modified Poulton solution with the composition described on Appendix B2.

3.5.1. Macrostructure analysis

The objective of the macrostructure analysis is to estimate the average ratio between the material used to manufacture a part and the total usable material. The ratio is obtained by the volume relation of the AM wall after fabrication and after a possible machining operation. Instead of machining, the ratio calculations were made with an image software in order to estimate these values. The steps followed were:

- Calculate the electrode weight deposited;
- Insert a rectangle on the section of the wall and calculate the area, determining the useful area;
- The calculated area is multiplied by the length of the wall and the alloy density, obtaining the useful mass;
- Knowing the mass deposited and the useful mass, the Useful Mass Ratio (UMR) is calculated.

The equations used were:

$$UMR = \frac{m_{useful}}{m_{deposited}} \times 100\% \quad (8)$$

$$m_{deposited} = m_{substrate+deposit} - m_{substrate} \quad (9)$$

$$A_{useful} = w_{useful} \times h_{useful} \quad (10)$$

$$m_{useful} = (A_{useful} \times l_{wall}) \times \rho_{alloy} \quad (11)$$

$$UMR = \frac{m_{useful}}{m_{deposited}} \times 100\% \quad (12)$$

3.5.2. Microstructure analysis

In the microstructure analysis the main objective was to determine the average grain size, verify the existence of the precipitates and defects found in the NDT.

The surface preparation as described in Appendix B is crucial in order to analyze the microstructure. The steps followed in this stage of the work were:

- Sample preparation;
- Grinding and polishing;
- Etching;
- Light Optical Microscopy (LOM) analysis, in order to verify the success of the etching and calculate the average grain size;
- Scanning Electron Microscopy and Energy Dispersive Spectroscopy (SEM/EDS) was executed in order to analyze the microstructure in detail, especially if precipitates were formed and to obtain a chemical composition of those.

3.6. Hardness

In this work in order to analyze the mechanical properties of the parts manufactured, a Vickers hardness test was performed. This is a method to measure the hardness of materials which is easier to use than other hardness tests since the required calculations are independent of the size of the indenter. In this test the indenter can be used for all materials because it's a diamond pyramid indenter, as shown in figure 3.15.

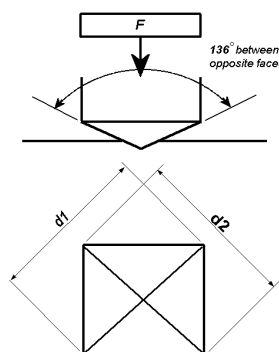


Figure 3.15: Hardness test principle illustration

The test was performed using a load of 5N during 15 seconds. Twenty five indentations on each sample were performed along the AM wall section. The procedure was executed according to the standard ISO-6507-1 (Appendix C)

This test was performed on the *Duramin Struers-1/-2* and the main equations used to calculate the hardness are:

Area:

$$A = \frac{d^2}{2 \times \sin\left(\frac{136}{2}\right)} = \frac{d^2}{1.8544} \quad (13)$$

$$d \text{ [mm]} = \frac{(d1+d2)}{2} \quad (14)$$

Hardness Vickers:

$$HV = \frac{F[\text{Kgf}]}{A \text{ [mm}^2]} \leftrightarrow HV = \frac{1.8544 \times 5 \times 10^5}{\left(\frac{(d1+d2)}{2}\right)^2} \quad (15)$$

Average Hardness:

$$\text{Average HV} = \frac{\sum HV}{\text{Number of indentations made in the weld}} \quad (16)$$

4. Results and Discussion

In this chapter the results are presented and discussed, regarding metallographic and mechanical analysis.

4.1. Deposition Efficiency and Heat Input

In order to calculate the process efficiency some steps were followed primarily to obtain the process efficiency indicators.

The main indicators to study in this work are the deposition efficiency and the heat input. The deposition efficiency regards the amount of material deposited in the substrate plate determining if the deposition rate is attractive to adopt in AM applications. Heat input it is directly implied in the metallurgical properties of the walls and combined with the deposition efficiency allows determining the optimal parameters to build walls, and necessarily the welding procedure that should be adopted.

4.1.1. Wall build up

The walls were built as described in chapter 3, analysing the layer deposition that forms the walls.



Figure 4.1: Test part 130A



Figure 4.2: Test part 120A



Figure 4.3: Test part 110A



Figure 4.4: Test part 100A



Figure 4.5: Test part 90A



Figure 4.6: Test part 80A

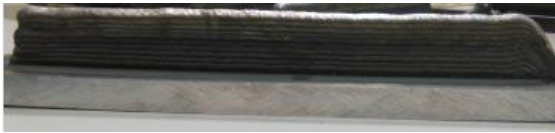


Figure 4.7: Test part 70A



Figure 4.8: Test part 60A

The images above correspond to the parameter current intensity: 130A, 120A, 110A, 100A, 90A, 80A, 70A and 60A.

4.1.2. Voltage and Current average calculations

The parameters chosen to build the AM walls were set in the *Fronius* controller but those values are average values, given in the controller display. So, in order to obtain the real values of voltage and current, a data acquisition system was used for acquiring the real values, measured instantly during the welding process and then with the acquired data the calculations of the average current and voltage were made.

The calculations were based on the waveform obtained by the DAQ system, shown in the Figure 4.9:

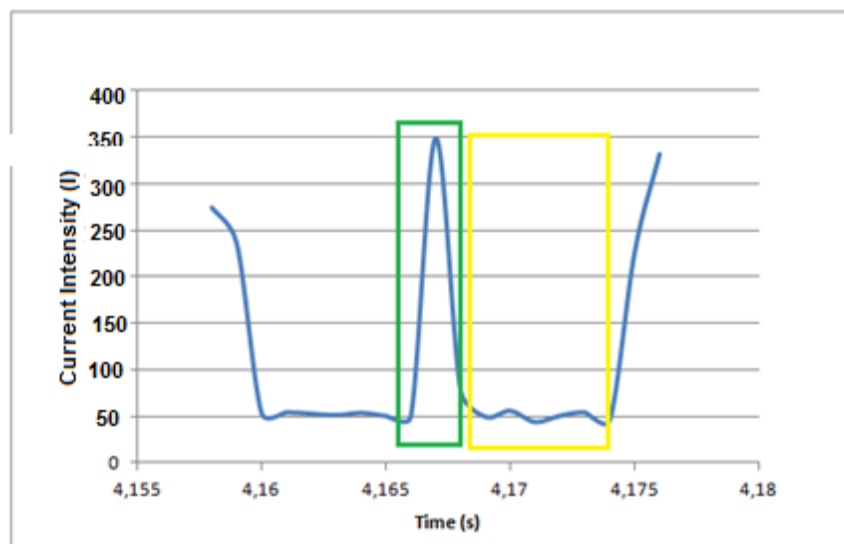


Figure 4.9: Waveform for current in CMT operation cycle for 90A sample

There are two phases to analyse in the Figure 4.9, the arcing phase isolated in the green rectangle and the short circuiting phase shown in the yellow rectangle. For the voltage the obtained waveform is shown in the Figure 4.10:

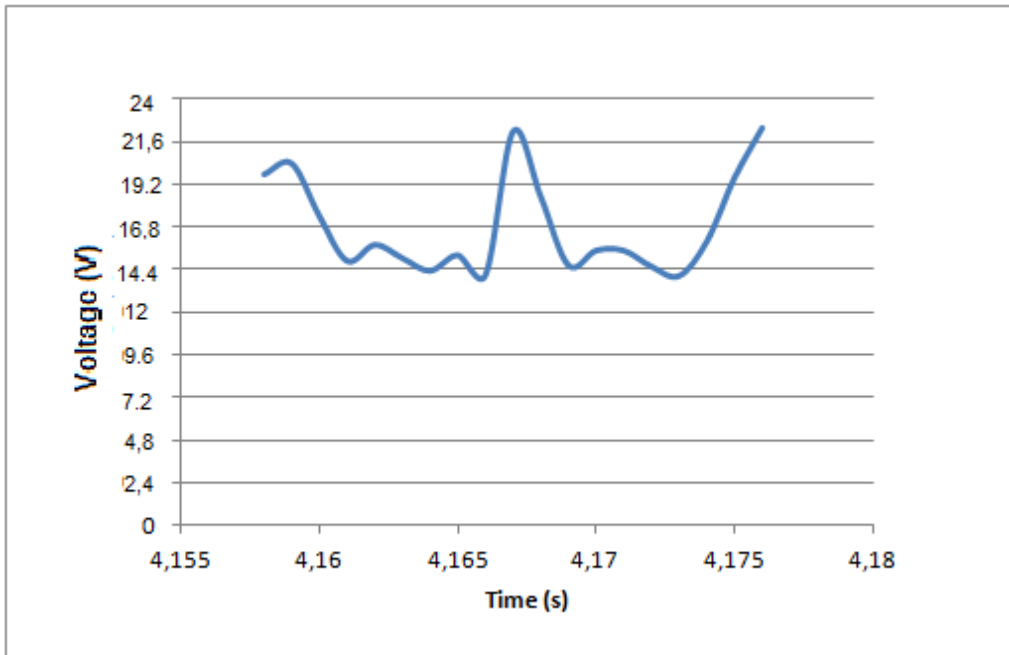


Figure 4.10: Voltage Waveform in CMT operation cycle for 90A sample

In both current and voltage, the values obtained of the DAQ system should be converted in to real values, so in order to convert, each quantity it is multiplied by a coefficient. The coefficients are 100 in the current case and 24 in the voltage case.

For both parameters the approach used to calculate the average values were the same that was [105]:

$$\bar{V} = \frac{\frac{t_1(V_p - V_b)}{2} + t_2(V_p - V_b) + \frac{t_3(V_p - V_b)}{2} + V_b(t_b + t_p)}{(t_b + t_p)} \quad (17)$$

$$\bar{I} = \frac{\frac{t_1(I_p - I_b)}{2} + t_2(I_p - I_b) + \frac{t_3(I_p - I_b)}{2} + I_b(t_b + t_p)}{(t_b + t_p)} \quad (18)$$

The equations used assume that the waveform has a trapezoidal form, and the expressions correspond to the area above the graph, meaning that:

$$V_i = \int_0^T V_i(t) dt \quad (19)$$

$$I_i = \int_0^T I_i(t) dt \quad (20)$$

The steps followed for these calculations were:

- Determine the I_b , I_p , t_b , t_p and $t_{1,2,3}$;
- Calculate the values by the Equations;
- Use the calibrations for the transducers to transform the calculated values in to real values, these calibrations are expressed in the equipment itself (Figures 4.11 and 4.12). 1V corresponds to 100A for current measuring and for Voltage measuring the relation is that 5V measured correspond to 120V, implying the ratio is 1:24.



Figure 4.11: Calibration coefficient for Current DAQ



Figure 4.12: Calibration coefficient for Voltage DAQ

The calculations for the average values used for the wall build ups are expressed in the following table (Table 4.1):

Test Part	Average Current (A)	Average Voltage (V)	Travel speed (mm/min)	Wire Feeding Rate (m/min)	Gas Flow Rate (L/min)	Number of Layers
130A	166.2	23.4	600	11.4	17	20
120A	171.7	19.9	600	10.4	17	22
110A	135.7	20.2	600	9.3	17	22
100A	133.3	17.8	600	8.5	17	24
90A	110.9	15.9	600	7.6	17	24
80A	101.0	18.3	600	6.8	17	24
70A	85.3	15.2	600	6.0	17	26
60A	71.7	15.6	600	5.2	17	26

Table 4.1: Parameters obtained for each test part

All the parameters were acquired to perform the deposition efficiency and heat input calculations.

4.1.3. Deposition Efficiency and Heat Input

The deposition efficiency determination, described in the chapter 3, it is shown in the Table 4.2:

Test Part	Weight of electrode used (g)	Substrate plate weight (g)	Substrate plate + Deposit (g)	Deposition Efficiency (%)
130A	396.53	466.9	795.3	82.81
120A	397.92	456.2	797.7	85.82
110A	355.83	484.6	761.5	77.81
100A	354.79	472.9	742.7	76.04
90A	317.22	489.8	738.5	78.39
80A	283.83	461.3	691.4	81.06
70A	271.31	478.1	706.3	84.10
60A	235.13	504.9	698.4	82.29

Table 4.2: Deposition efficiency and weights used for its determination

For the discussion of the results the focus will be on the relations between Current, Wire Feeding Rate, Deposition Efficiency and the Number of Layers. These measurements were chosen to analyse due to:

- Heat input affects the metallurgical and mechanical quality of the layers deposited;
- Wire feeding rate in GMAW process as direct influence in the current used to this process;
- Deposition Efficiency results on the ratio of consumed wire and deposited material, which is crucial to AM applications.

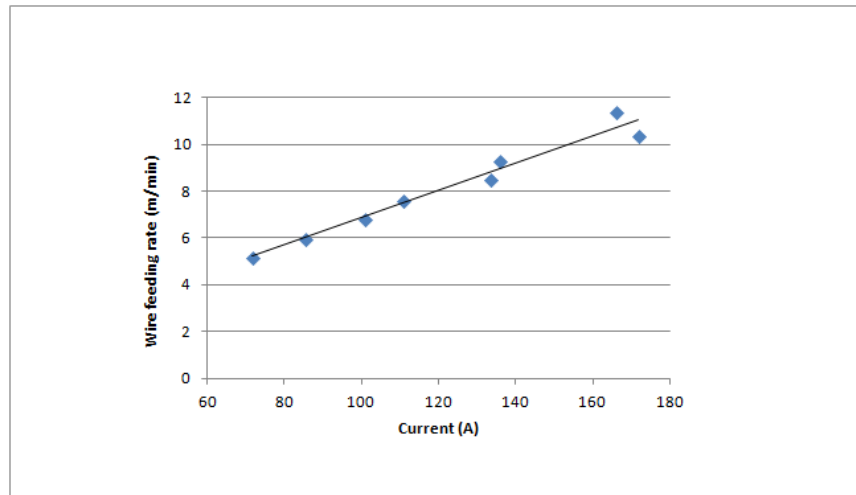


Figure 4.13: Relation between Wire Feeding Rate and current

The Wire Feeding Rate presents a linear relation with Current (Figure 4.14) and is directly proportional. Due to the low resistivity of the Aluminium not developing cathodic heat; [51], the following equation representing the wire melting rate, which is equal to the wire feeding rate in GMAW.

$$W = \alpha I + \beta I^2 \quad (21)$$

So according to the equation (21), the cathodic heat is represented to the β that equals to zero, concluding that the wire feeding rate is directly proportional to the current intensity to the consumable wire used in this work.

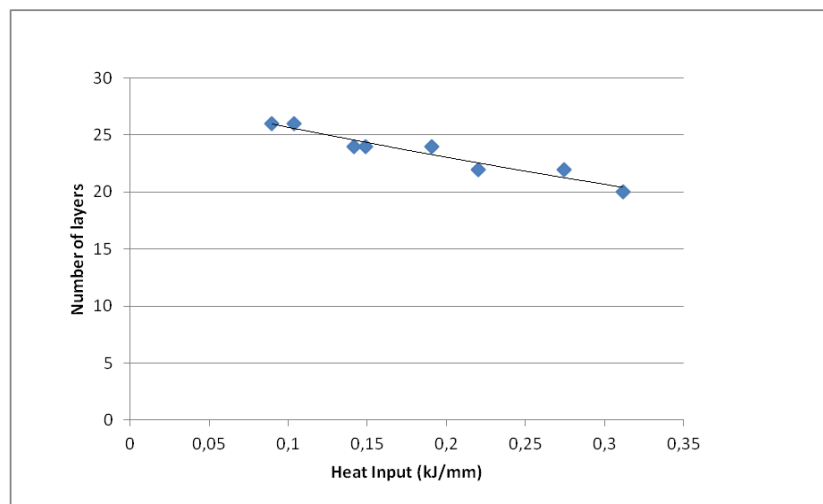


Figure 4.14: Relation between the number of layers and heat input

The Number of layers necessary to perform a wall is inversely proportional to the current (Figure 4.13) due to the characteristic adjustment of the CMT synergic control for the wire feeding rate, so if the current is higher the Number of layers needed to manufacture a part is lower. Knowing that current intensity is directly proportional to the heat input as expressed in equation (3), the number of layers is inversely proportional to the heat input as well.

For the Heat Input analysis the following table (Table 4.3) express the parameters used with the results obtained:

Test Part	Average Current (A)	Average Voltage (V)	Travel speed (mm/min)	Heat Input (kJ/mm)
130A	166.2	23.4	600	0.311
120A	171.7	19.9	600	0.274
110A	135.7	20.2	600	0.220
100A	133.3	17.8	600	0.190
90A	110.9	15.9	600	0.141
80A	101.0	18.3	600	0.1487
70A	85.3	15.2	600	0.103
60A	71.7	15.6	600	0.089

Table 4.3: Heat Input values and parameter used for its determination

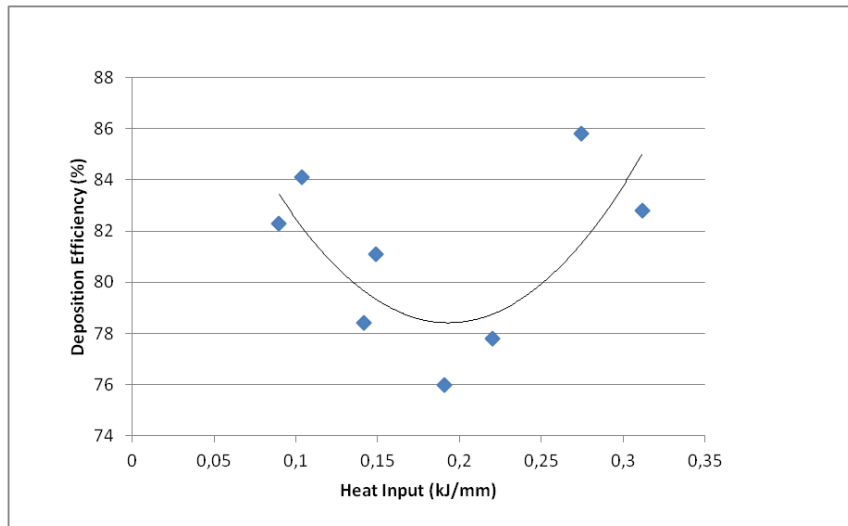


Figure 4.15: Graphic relation between Deposition Efficiency and Heat Input

The Deposition Efficiency presents a characteristic relation between both Heat Input and Current (Figures 4.15 and 4.16). The value distribution suggests a quadratic relation with 3 zones of interest to analyse, shown in the Figure 4.16:

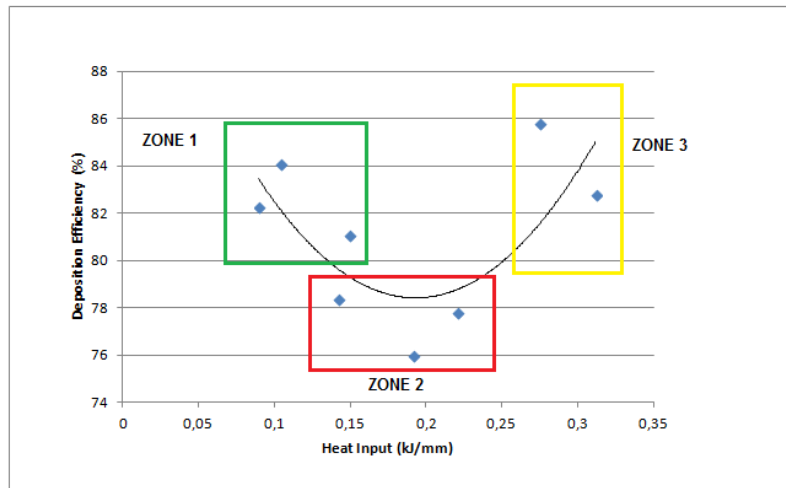


Figure 4.16:Relation between Deposition Efficiency and Heat Input

According to these 3 zones, the following can be considered:

- In the 1st Zone (green rectangle), the range of Values correspond to Currents between 70A and 100A, the metal transfer mechanism is characterized as short circuit transfer and the metal transfer it is stable allowing a smooth deposition of the droplets [102], this is an interesting operation domain to operate for AM;
- In the 2nd Zone (red rectangle), the Current range is between 110A and 135A, and the metal transfer mechanism is situated between the short circuit domain and the spray transfer domain [105], creating spatter and metal vaporization [102] [107], decreasing the deposition efficiency;
- In the 3rd zone (yellow rectangle), the range of values correspond to Currents between 165A and 170A and the transfer mode considered is the short circuit-spray transfer, which means that the deposition efficiency is higher that the but the Heat Input it is higher too [105].

Considering these results, the best welding procedure to adopt in the fabrication of AM parts are the 70A set of parameters because reunites high deposition efficiency associated to a low heat input, allowing saving energy in the process and diminishing residual stresses.

4.2. Macrostructure Analysis

The macrostructure analysis in this work was performed in order to determine the useful cross section area in each test part and to establish an approach concerning the mass usage in an AM part, as described in chapter 3.

The test parts used were the 130A, 110A, 80A and 60A because those can be representative in the parameter range used. The AM walls cross sections are shown in Figure 4.17.

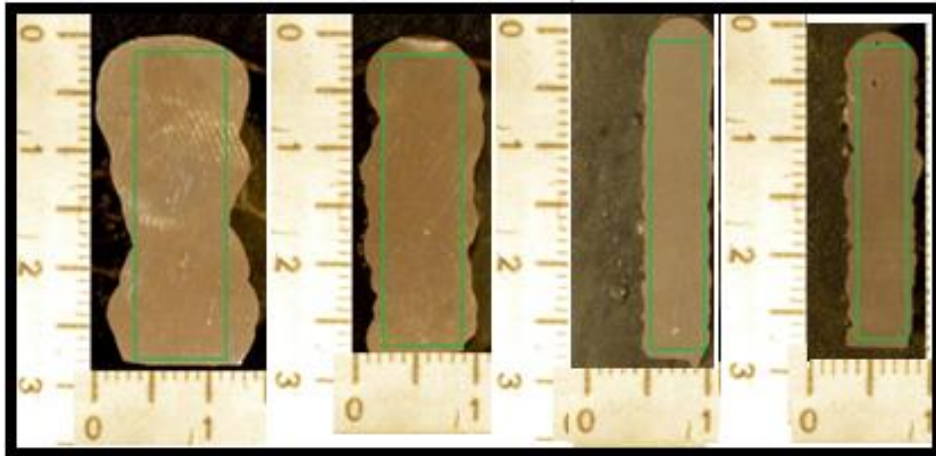


Figure 4.17: Useful area represented for parts 130A, 110A, 80A and 60 A respectively

The values of the useful areas, deposited mass, useful mass and UMR are expressed in the following table (Table 4.4):

Test Part	Useful Area (cm ²)	Useful mass (g)	Deposited Mass (g)	Weight of eletrode used (g)	UMR (%)
130A	2.12	140.45	328.4	396,53	44,38
110A	2.25	149.0625	276.9	397,92	45,21
80A	1.82	120.575	230.1	355,83	56,43
60A	1.56	103.35	193.5	354,79	42,79

Table 4.4: UMR calculations and values used for its calculation

The relation concerning the UMR with the number of layers, deposition efficiency, the heat input, and weight of electrode used shown in the following Figures 4.18, 4.19, 4.20 and 4.21.

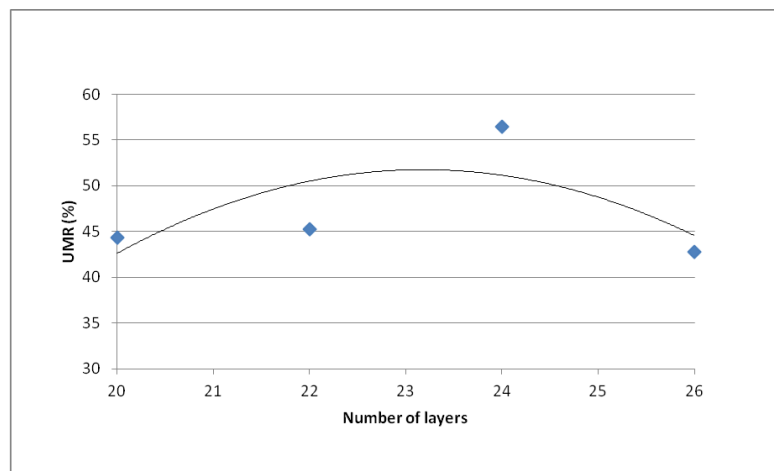


Figure 4.18: Relation between UMR and the number of layers

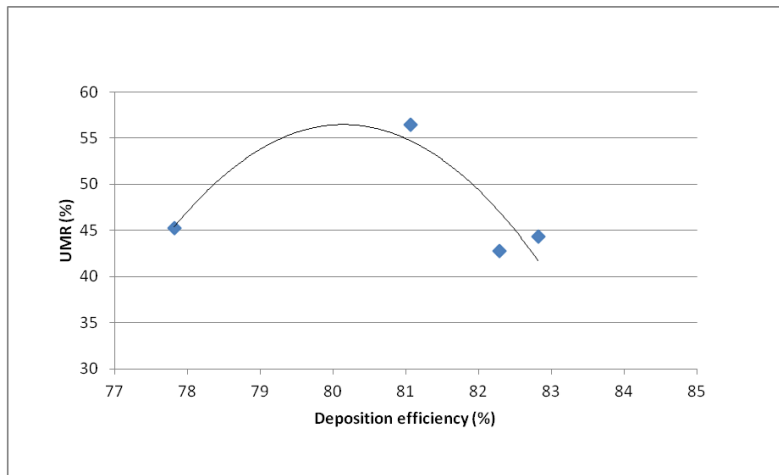


Figure 4.19: Relation between UMR and the Deposition Efficiency

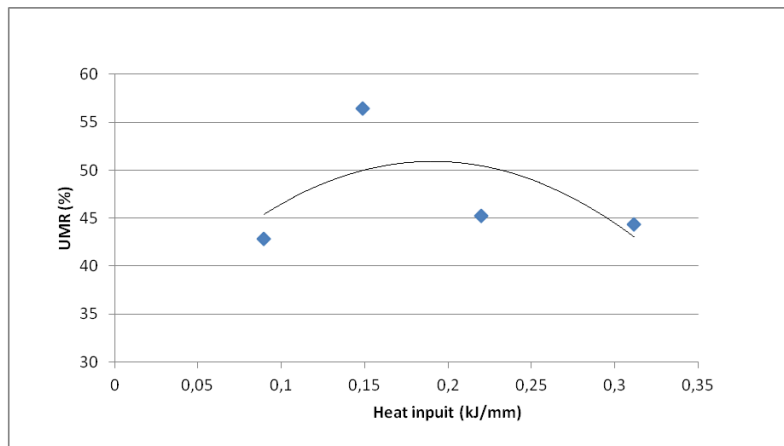


Figure 4.20: Relation between UMR and Heat Input

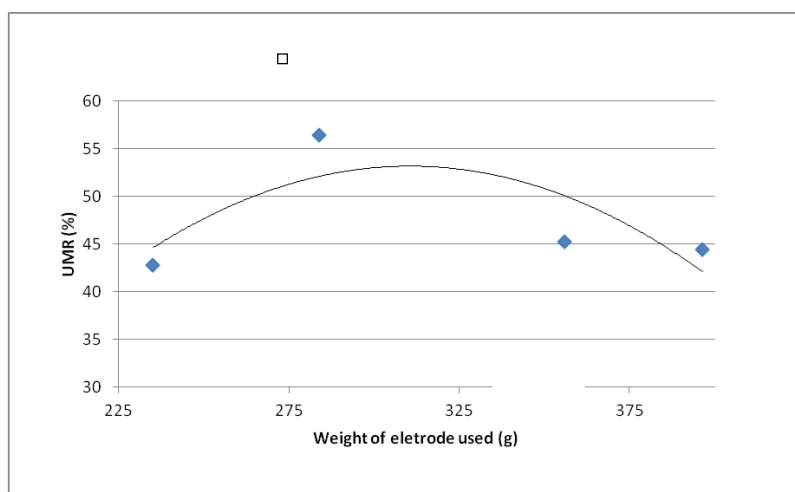


Figure 4.21: Relation between UMR and Weight of eletrode used

These results obtained on this procedure allow concluding that:

- The combination of conditions that showed the best results in this work, concerning the UMR, are 100A of Current, approximately 148 J/mm of Heat Input, 81% for deposition efficiency and 24 layers of the AM wall build up;
- The number of layers that represents the best Useful Mass Ratio are 24, corresponding to the Current range of high deposition efficiency and low heat input shown in the chapter 4.1.3;
- The deposition efficiency graph corresponds to a polynomial function, and the inflexion zone represents the transition from short circuit transfer to spray transfer, meaning that the transition of transfer mode affects the metal deposition due the arc instability that occurred [7];
- The heat input corresponds to a polynomial function too, the implications of the heat input on the UMR are:
 - For low heat input the layers melted zone will be not sufficient, creating poor fusion between layers;
 - For high heat input occurs good fusion between layers;

The heat input is proportional to the mass of material fed to build an AM wall, in the best result obtained, the ratio between heat input and wire feeding speed it is well balanced in order to promote weld bead geometry capable to assemble several layers and assure good fusion between them [108].

4.3. Hardness

The hardness tests performed in this work were made in order to evaluate the mechanical properties of the AM walls and predict metallurgical aspects.

The hardness tests performed along the AM wall sections of test parts 130A, 110A, 80A and 60A, using the following the procedure described in the chapter 3, and the indentations are shown in figure 4.22:

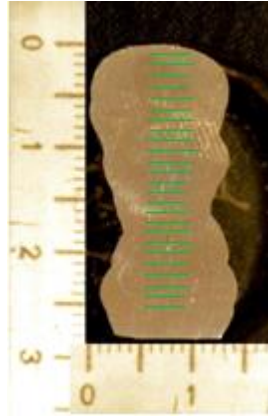


Figure 4.22: Hardness test patterns applied in all test part sections

The results obtained are expressed in figures above (Figures 4.23, 4.24, 4.25 and 4.26):

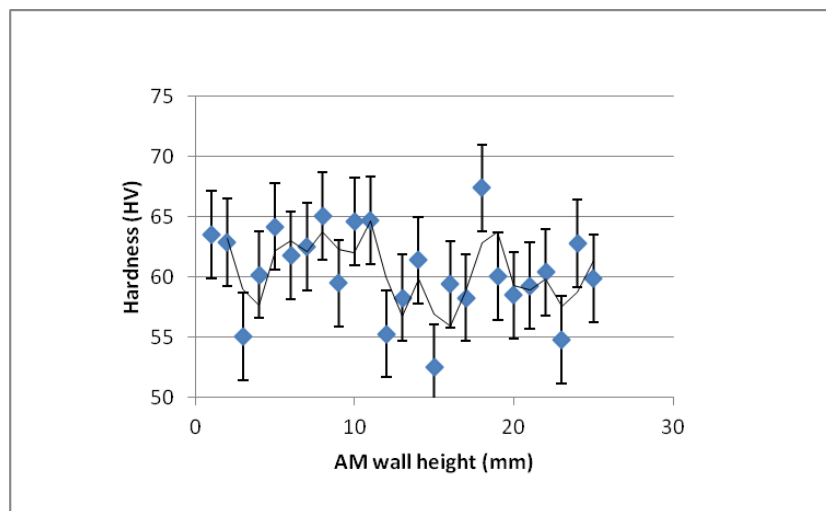


Figure 4.23: Hardness distribution along the section of 130A test part

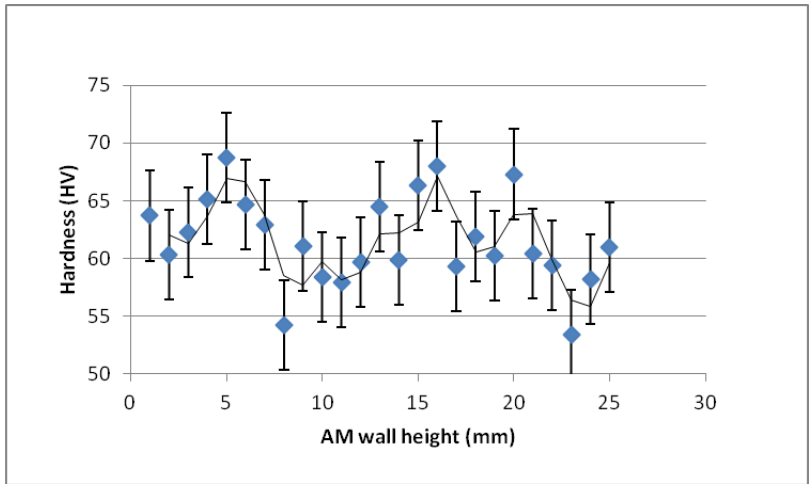


Figure 4.24: Hardness distribution along the section of 110A test part

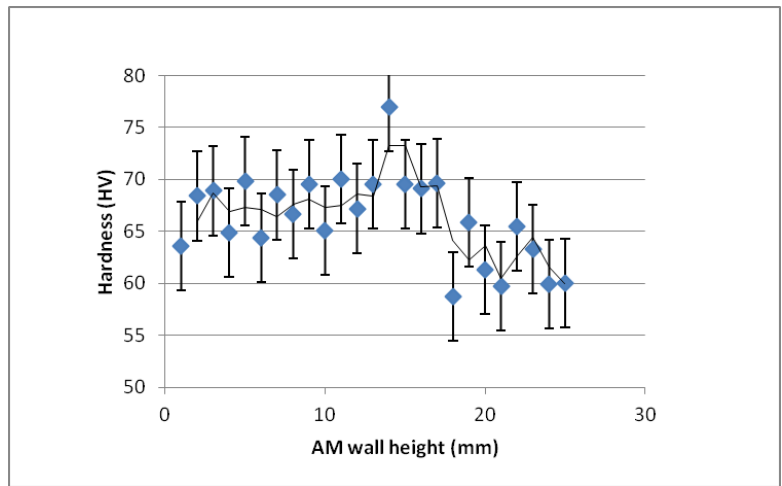


Figure 4.25: Hardness distribution along the section of 80A test part

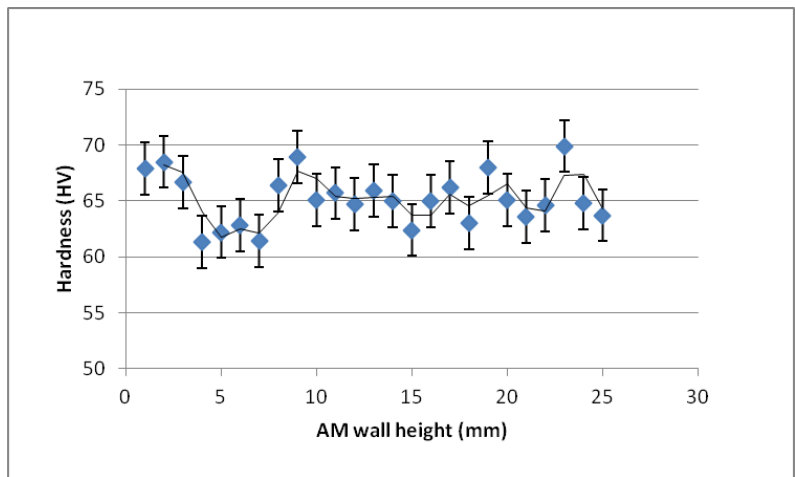


Figure 4.26: Hardness distribution along the section of 60A test part

Test part	Heat Input (J/mm)	Average Hardness (HV)
130A	0.311	60±3.6
110A	0.220	60.7±3.8
80A	0.148	66.2±4.2
60A	0.089	64.9±2.3

Table 4.5: Average Hardness of each test part

In all samples exists a small deviation from the average hardness value but the hardness is almost the same in all samples, allowing to conclude that the mechanical properties are homogeneous in all the samples (Table4.5), despite variations of the Heat Input.

Considering that the nearest average hardness value of the aluminium alloy 5083 is in “O” state is 87HV [106], corresponding to a thermal cycle of annealing and recrystallization, the average values obtained are above this value [109].

Assumptions regarding the average grain size and quantity of precipitates formed during the process can be made, but the metallographic analysis will determine those aspects allowing to achieve solid conclusions.

All values point that the mechanical properties are homogeneous along the AM wall section.

4.4. Microstructure analysis

This microstructure analysis consists on microscopy techniques in order to obtain the microstructure, grain size, verify the existence of precipitates and the chemical composition.

After executing the procedure described in the Appendix B1, using the Keller solution, other approach was taken by using the modified Modified Poulton solution. The Keller solution it is used mainly to highlight the precipitates formed in the alloy, the Modified Poulton solution is used to differentiate the grain microstructure and the recrystallized grains.

The results with the Keller solution are represented in the following figures (Figure 4.27, 4.28, 4.29, 4.30, 4.31, 4.32, 4.33 and 4.34):

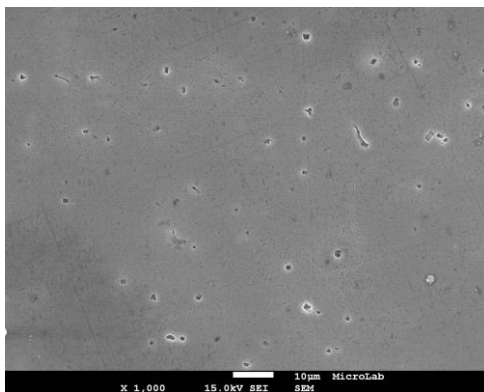


Figure 4.27: SEM image captured from the 130A test part with 1000x magnification

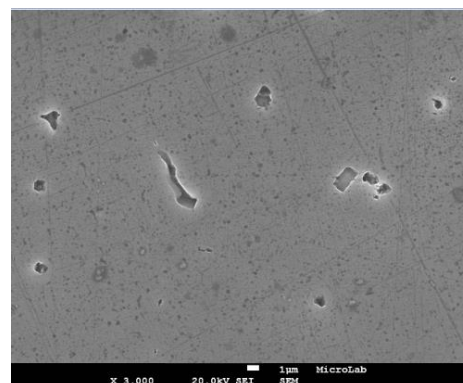


Figure 4.28: SEM image captured from the 130A test part with 3000x magnification

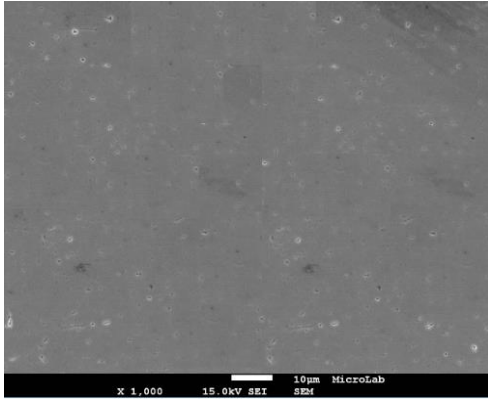


Figure 4.29: SEM image captured from the 110A test part with 1000x magnification

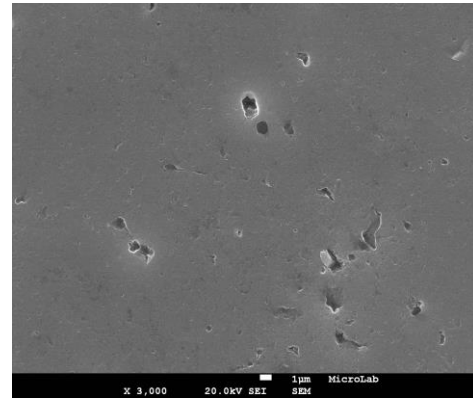


Figure 4.30: SEM image captured from the 110A test part with 3000x magnification

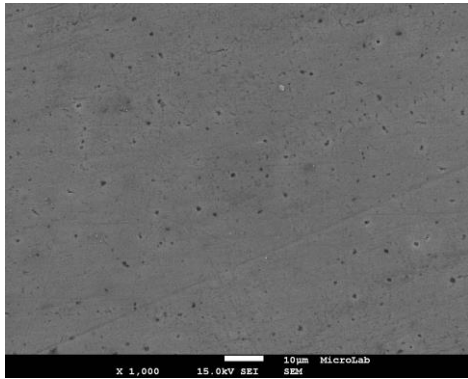


Figure 4.31: SEM image captured from the 80A test part with 1000x magnification

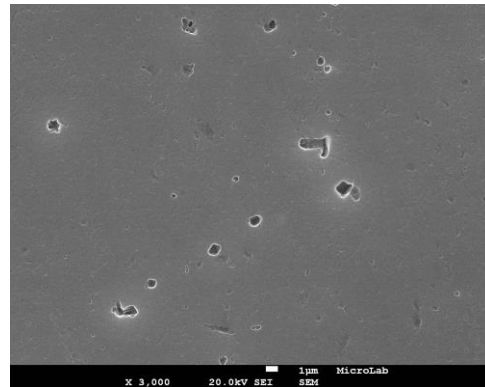


Figure 4.32: SEM image captured from the 80A test part with 3000x magnification

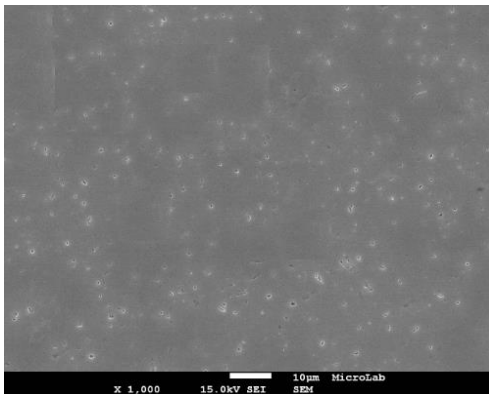


Figure 4.34: SEM image captured from the 60A test part with 1000x magnification

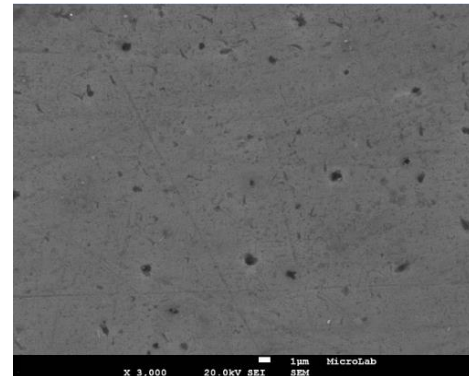


Figure 4.33: SEM image captured from the 60A test part with 3000x magnification

These pictures that were captured with the Keller solution etching but were not possible to etch with the purpose to reveal the microstructure because of the characteristic of this aluminium alloy, of the 5xxx series, which is the corrosion resistance [97]. The EDS analysis could be executed in order to differentiate the chemical composition of the dark zones from the bright zones that appeared in the surface scanning. The chemical compositions are represented in table 4.6:

Weight percentage	Bright Zone		Dark Zone	
	Al (w %)	Mg (w %)	Al (w %)	Mg (w %)
130A	93.35	6.65	93.32	6.68
110A	92.93	7.07	91.18	8.82
80A	92.87	7.13	93.54	6.46
60A	94.61	5.39	91.12	8.88

Table 4.6: Chemical composition obtained in the EDS analysis, for each test part, concerning the zones of interest.

After performing these tests, the samples were polished and etched with Modified Poulton solution in order to highlight the microstructure of the alloy. After highlighting the microstructure, the objective is to determine the average grain size.

The approach used in the average grain size was the Heyn method [110] which consists in counting 50 grains in a row and measure each one of them in order to determine the average.

The microstructure images captured were made with 50x magnification and are shown in the following Figures 4.35, 4.36, 4.37 and 4.38:

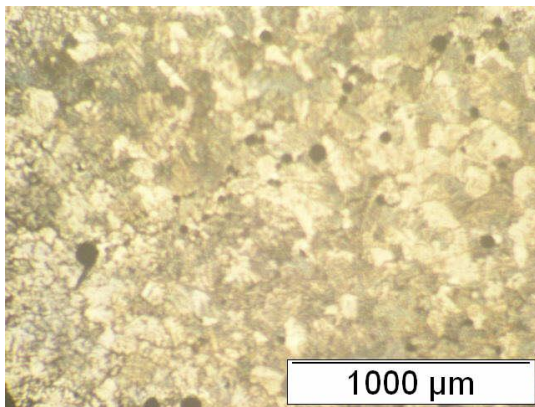


Figure 4.35: 130A test part microstructure with 50x magnification.

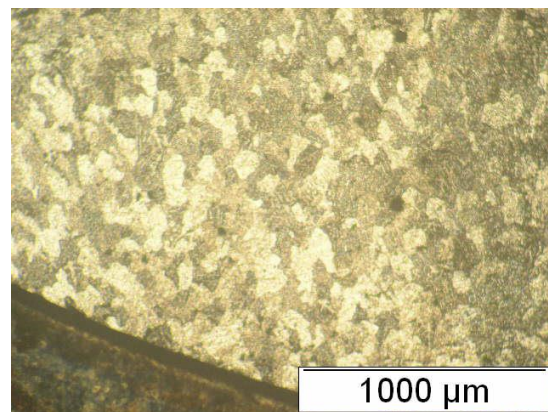


Figure 4.36: 110A test part microstructure with 50x magnification.

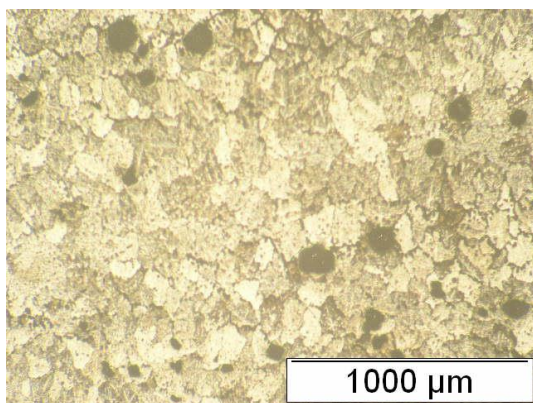


Figure 4.37: 80A test part microstructure with 50x magnification.

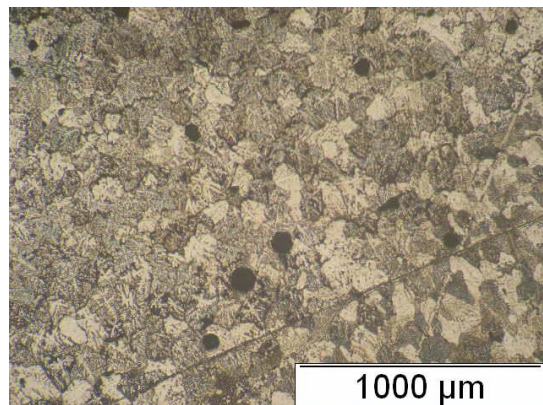


Figure 4.38: 60A test part microstructure with 50x magnification.

The following table (Table 4.7) shows the average grain size with the respective deviation:

Test part	Average grain size (μm)
130A	$152 \pm 59 \mu\text{m}$
110A	$157 \pm 60 \mu\text{m}$
80A	$154 \pm 56 \mu\text{m}$
60A	$161 \pm 51 \mu\text{m}$

Table 4.7: Average grain size for each test part

The average grain size in these samples suffered the same heat treatment that was successive heating and cooling stages. This thermal cycle applied promotes the grain growth and consequently an average grain size that is consistent with the hardness values and is uniform in all samples.

In these samples some pores were found. Pores are a common defect that can be found in welds. In order to validate the AM wall integrity the size and pore fraction were calculated by using a image treatment, *ImageJ*.

The images captured were treated in order to highlight the pores in the sample surface, as shown in the figures 4.39, 4.40, 4.41 and 4.42:

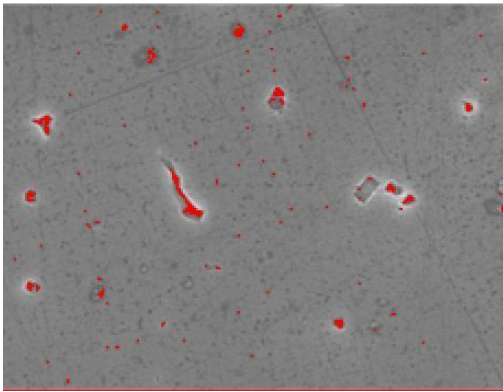


Figure 4.39: 130A test part with 3000x magnification with the pores highlighted

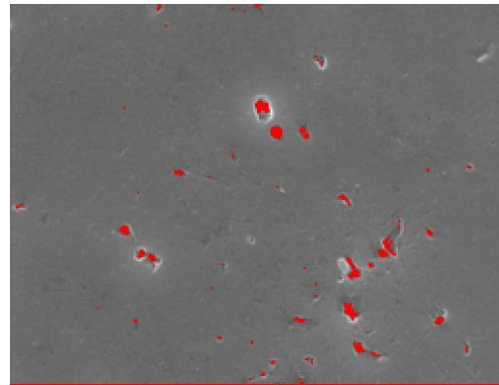


Figure 4.40: 110A test part with 3000x magnification with the pores highlighted

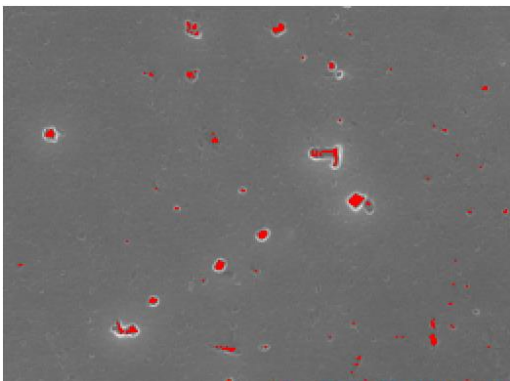


Figure 4.41: 80A test part with 3000x magnification with the pores highlighted

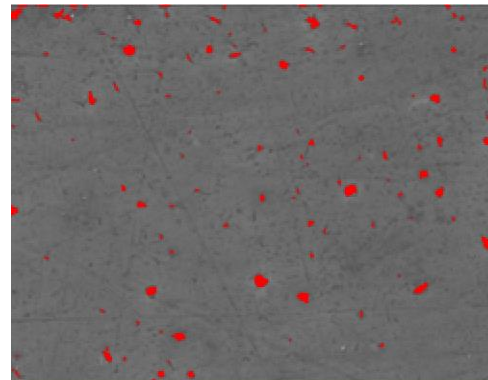


Figure 4.42: 60A test part with 3000x magnification with the pores highlighted

The results obtained in this brief analysis are expressed by direct data given into *ImageJ*, represented in the following table:

Test part	Test sample area (μm^2)	Average size (μm)	Pores/Sample area (%)
130A	4433	0,057	0,428
110A	4195	0,079	0,416
80A	4589	0,063	0,411
60A	5124	0,048	1,165

Table 4.8: Porosity analysis considering the occupied area and average size

After these tests performed the conclusions made are:

- It was expected to find precipitates in the microstructure of the aluminium, but due the thermal cycle applied , associated with the welding process, precipitates were not formed [109];
- The SEM and EDS analysis allowed to determine the pores formed during the solidification of the alloy. The chemical composition in the dark zones (pores) is nearly the same that in the bright zones;
- The grain size and the lack of precipitates is consistent the average hardness obtained [109].
- The porosity found in the samples does not compromise the mechanical properties because the pore percentage is way low. The preventive measures suggested are [111]:
 - Degrease the surfaces with volatile solvents;
 - Use a wire brush for cleaning after the layer deposition, and the wire brush must be a stainless steel wire brush;
 - Chemical treatment of the surface with alkaline or acid solutions.

4.5. Non Destructive Testing

In this chapter the results obtained in the Non Destructive Tests are presented, on the test parts manufactured at Instituto Superior Técnico and Cranfield University in order to compare with the destructive test results and achieve conclusions about the potential of application of UT in AM.

4.5.1. Phased Array Ultrasound Testing

The PAUT testing was the first technique used for comparison with other techniques.

These test parts were different from each other specially the dimensions. The table 4.9 presents the dimensions for each part tested.

Part number	Thickness (mm)	Width (mm)
1	20	24
2	17	24
3	14	24
4	14	20
5	9	19
6	9	9
7	10	12
8	15	12
9	14	12
10	17	18
11	18	14

Table 4.9: AM steel parts dimensions

These parts correspond directly to the ones in Figure 4.43:



Figure 4.43: AM steel parts with the respective indication number

The results obtained in this work are represented on a series of zones that were the most relevant for the inspection of manufactured parts. The defects that can be considered as typical or major are the ones that present a signal intensity of 20% or higher, shown on the A-Scan.

The Figure 4.44 represents the layout of the Multi 2000 software, which was used to the PAUT result analysis.

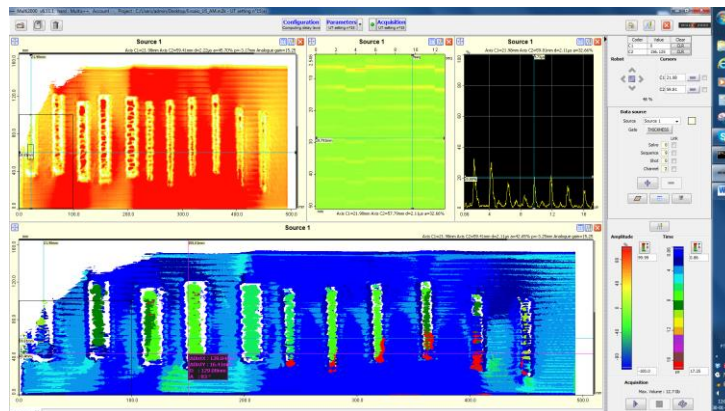
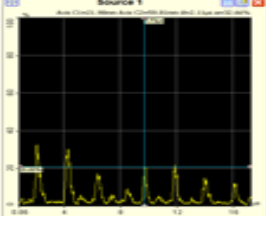
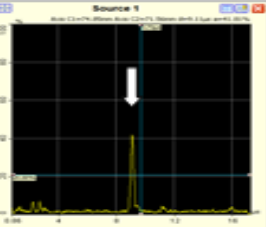
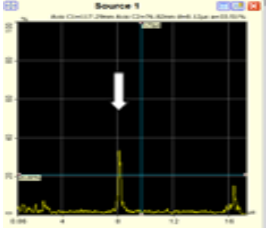
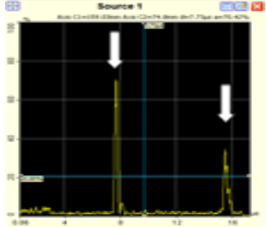
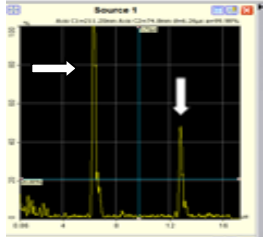


Figure 4.44: Multi 2000 software display

Considering that the ultrasound NDT process cannot be applied to an irregular surface, the analysis and scan were made through the back of the plate. All the peaks shown on the A-Scan up to 6,5mm must be ignored, since they represent defects on the substrate plate. The representative defects are shown on the A-scan, indicated with white arrows, considering the depth/thickness of the AM parts individually.

The table 4.10 indicates the A-scans and the commentaries for each part.

Part Number	A-Scan	Commentary
1		Near the limit of the plate the scan was not so effective but the analysis made on the part shows several defects, represented by the reflections black screen (A-Scan) , regarding the distance travelled vs the signal intensity correspondent to the echos received, and the relevant ones are at 10mm and 12mm with intensities near 20%.
2		This part was fully scanned and presented a defect at 9mm thickness with signal intensity about 40%.
3		This part presents a defect that on a thickness about 8mm with a intensity near 35%.
4		This part presents a major defect near 8mm thickness with intensity near 70% and near 16mm with 35% signal intensity.
5		This part presents defects near the interface with the substrate plate (t=6,5mm) with signal intensity of 100% and at near t=12mm with 50%.

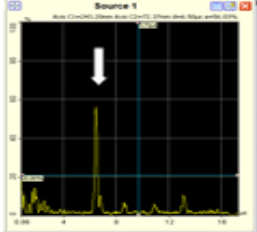
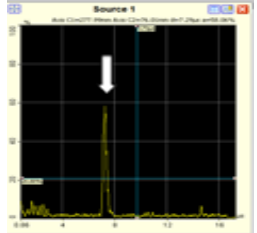
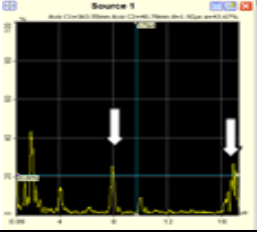
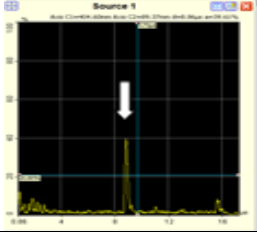
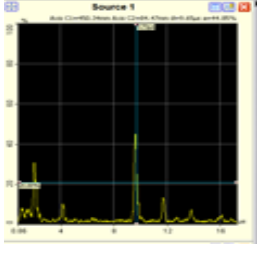
6		Presents a defect near the interface plate/part, similar to the part 5, but no defects are observed in the AM wall.
7		The considerations for this part are the same that were made in part 6.
8		No defects.
9		Presents some defects near t=8mm with 25% intensity and at the bottom of the part, t=17mm, with 25% intensity.
10		Presents a defect near t=9mm with 40% signal intensity.
11		Presents defects in two different regions of the part, first at t=8mm with almost 50% signal intensity (first A-Scan) and at the bottom of the part presents defects regarding the substrate plate (second A-Scan).

Table 4.10: Summary table of the PAUT analysis

The results obtained allow concluding that:

- The PAUT nondestructive test method can be applied at Additive Manufactured parts;
- The analyzed cases, the AM walls were small thus limiting the lateral movement of the probe. This led the lower accuracy of the results in the thinner walls;
- The software data analyzed provided allows to locate the defect but does not reveal the type of defect or its dimension;

4.5.2. Pulsed echo Ultrasound Testing and Radiation Testing

In the analyzed parts, both for aluminium and steel parts, the results will be expressed mainly by the specters obtained and from those the values of interest will be analyzed and compared respectively with the X-Ray acquired.

In UT techniques, the defects that present a signal intensity of 20% or more are the ones that were considered on these work due to the severity of the defects.

The steel test parts were numbered in order to recognize the test results and they are represented in the following Figure (Figure 4.45):

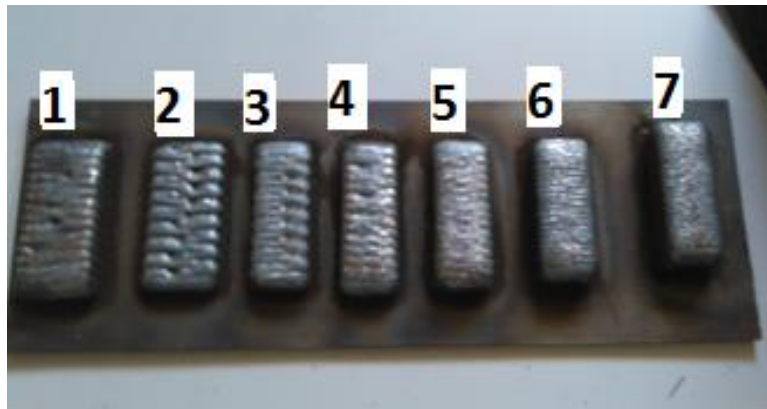


Figure 4.45: Steel parts for NDT testing numberd from 1 to 7

The dimensions associated to these parts are:

Part number	Thickness (mm)	Width (mm)
1	16	44
2	12	45
3	15	35
4	16	33
5	21	34
6	24	34
7	26	34

Table 4.11: AM steel part dimensions

The analysed aluminium part was the part with the 130A test conditions because was the only wall with considerable width to be tested with UT technique. The part dimensions are expressed in the Table 4.11:

Test Part	Thickness (mm)	Width (mm)
1A	15	10

Table 4.12: AM aluminium part dimensions

The IQI (Image Quality Indicator) scheme and the conditions for the radiation tests were the following:

Test Part Number	Aproximated Thickness (mm)	Minimum IQI	Maximum IQI	Voltage (kV)	Intensity (mA)	Distance from part (mm)	Time (min'seg)
1	24	W11	w13	200	3	700	3'
2	19	W11	w13	200	3	700	2'30
3	22	W11	w13	200	3	700	2'50
4	23	W11	w13	200	3	700	3'10
5	29	W10	w12	200	3	700	4'
6	31	W10	w11	200	3	700	4'20
7	33	W10	w11	200	3	700	5'
1A	39	W9	W12	120	3	700	1'

Table 4.13: X-Ray testing conditions and IQI obtained



Figure 4.46: UT spectre for the steel test vs. X-Ray part 1

The first part presents several defects that are detected by the X-ray and the UT (Figure 4.46). In the UT spectre, between the two gates (red bar and the green bar) that appear in all cases, we can ensure that:

- There is lack of fusion between the test part and the substrate plate, showed by the first echo at 6,27mm, that is the plate thickness;
- The other two defects occurred between the two imposed limits are major defects because the echoes intensity are bigger than 25%, around 50%, and the last echo in the green bar is the back wall echo.



Figure 4.47: UT spectre for the steel test vs. X-Ray part 2

In this case the defects found in the UT spectre do not present the same intensity in the echoes because the part and the substrate plate are not welded to each other, promoting the signal losses and wave deflections. These phenomena do not allow obtaining an accurate signal intensity measurement of the echoes.

Although the soundwave was not totally deflected, as in part 1 and some of the ultrasound propagated through the part and retrieved some echoes, and one of them showed near 25% of intensity, as can be seen at Figure 4.47.

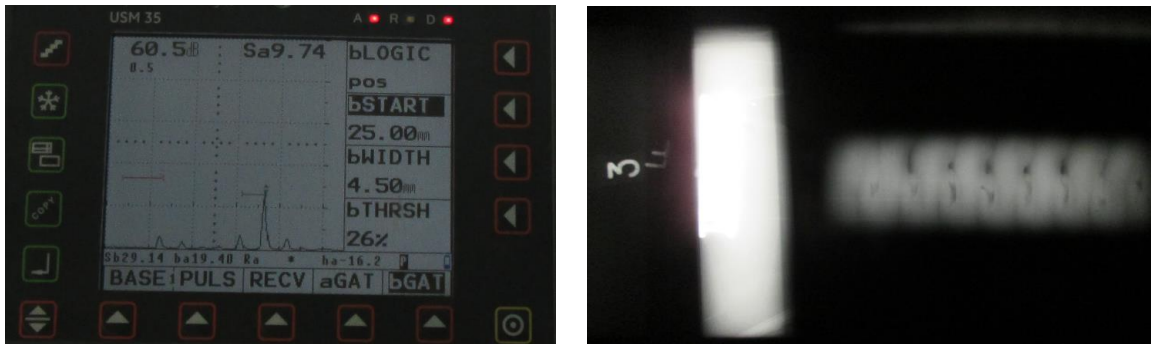


Figure 4.48: UT spectre for the steel test vs. X-Ray part 3

In this test part there were found some minor defects, fewer than 25% intensity, that the first echo is located at 9.74mm measured from the substrate plate surface (Figure 4.48). The X-Ray reveals other defects but the UT probe captured the defects in a brighter zone of the X-Ray film, due to a similar phenomenon that occurred in part 2.

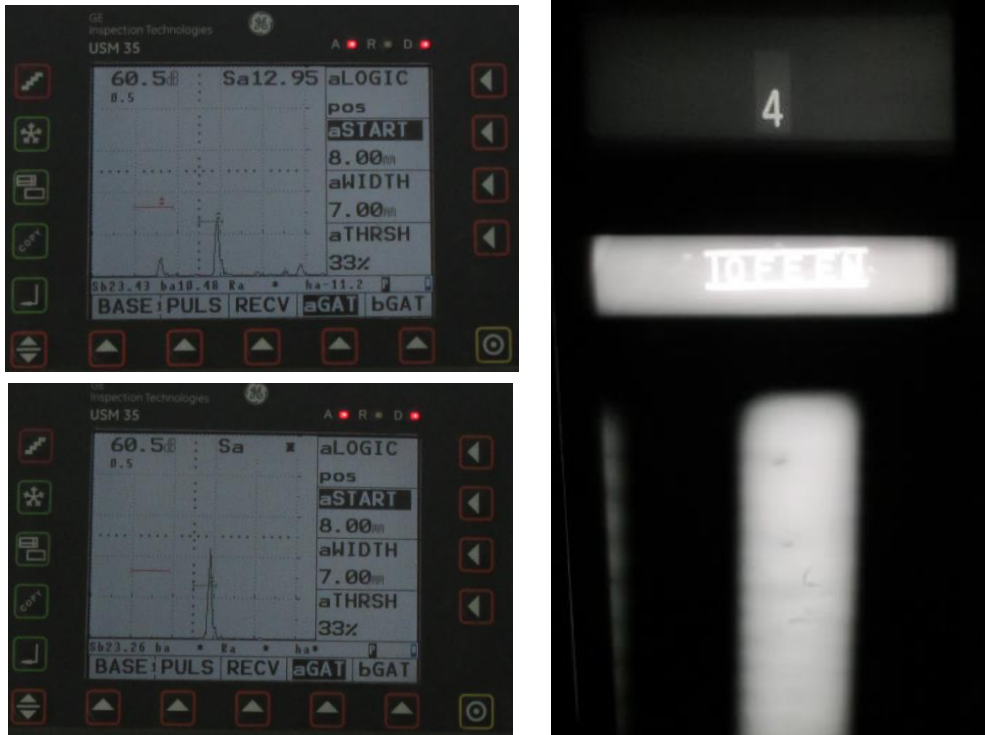


Figure 4.49: UT spectre for the steel test vs. X-Ray part 4

The test part 4 presents two distinguished zones with two different UT spectres as shown in Figure 4.49. The first spectre reveals a minor defect near the 12.95mm from the substrate plate surface with near 15% of intensity. The second spectre presents a no defect region, which can be confirmed by the X-Ray of the part.

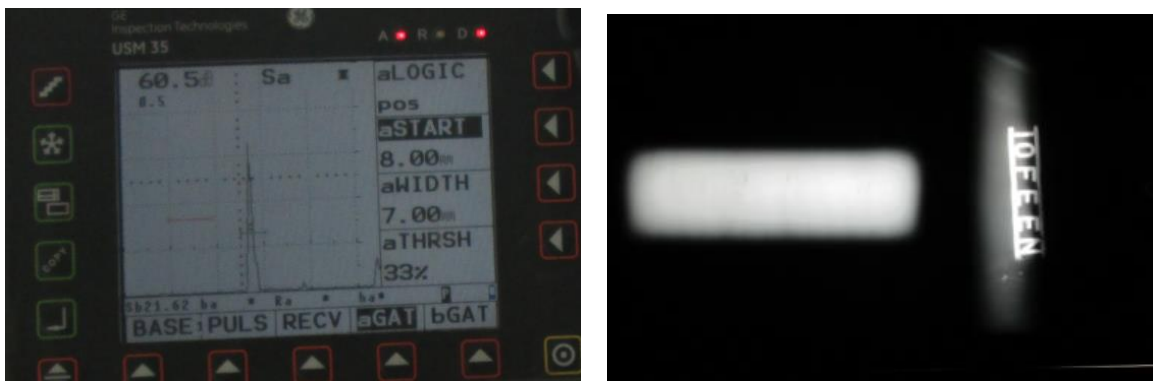


Figure 4.50: UT spectre for the steel test vs. X-Ray part 5

In part 5, both X-ray and UT spectre do not reveal any defects, as shown in Figure 4.50.

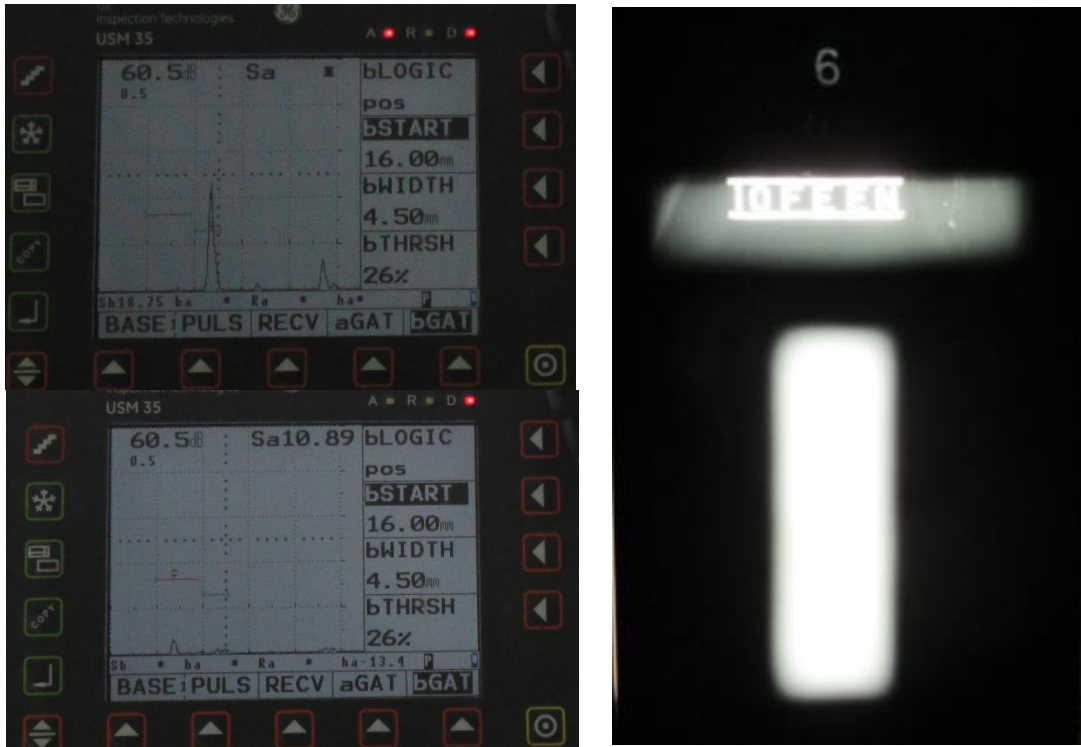


Figure 4.51: UT spectre for the steel test vs. X-Ray part 6

Test part 6 presents no defects, and the absence of back wall echo on the UT spectre in Figure 4.51 is explained as soundwave dispersion due to the irregularity of the opposed surface, corresponding to the maximum distance between the substrate plate surface and the wall thickness. These results are corroborated with a clean X-Ray.

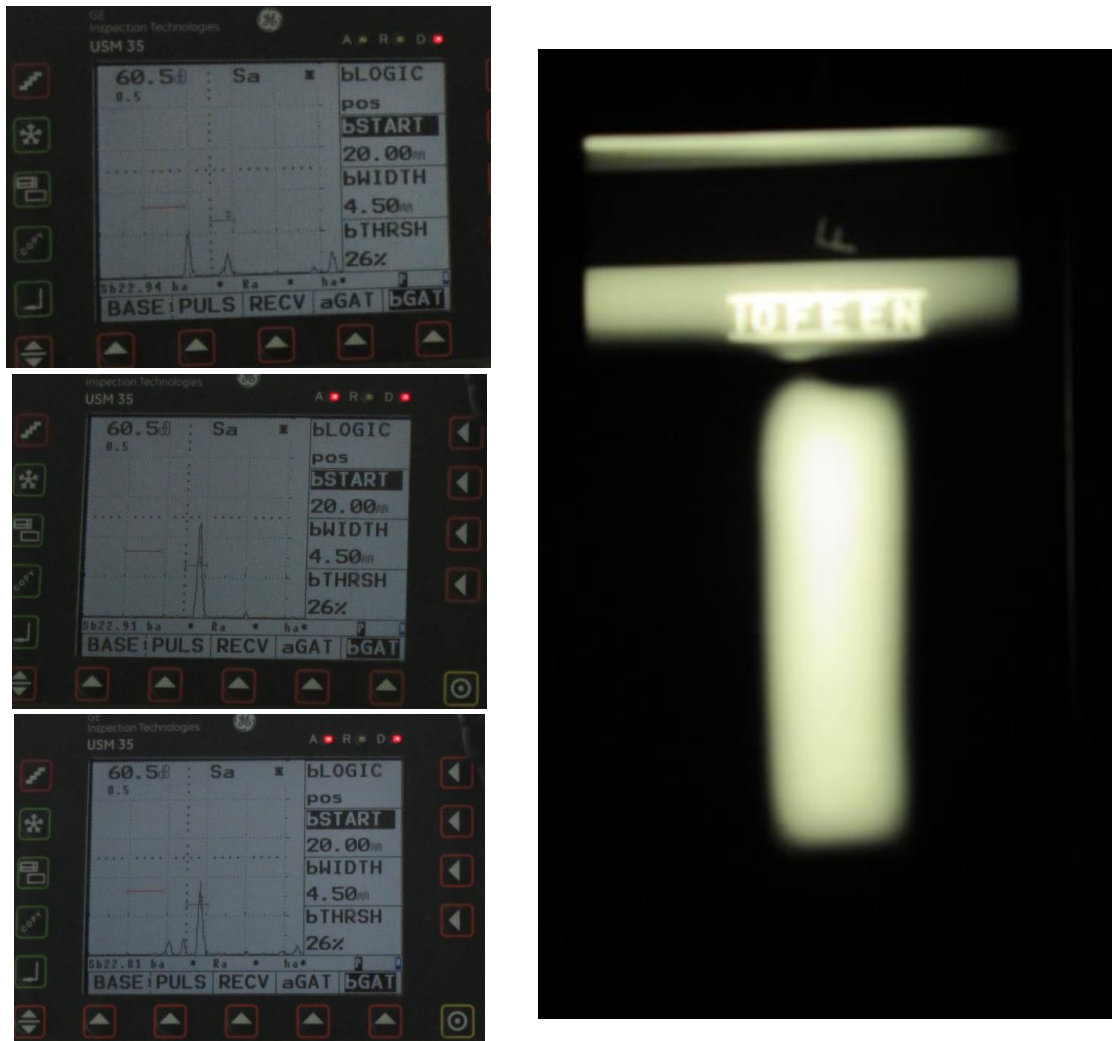


Figure 4.52: UT spectre for the steel test vs. X-Ray part 7

The last parts of steel analysed in this work, part 7, were found two minor defects in the UT spectre but do not appear in the X-Ray (Figure 4.52).

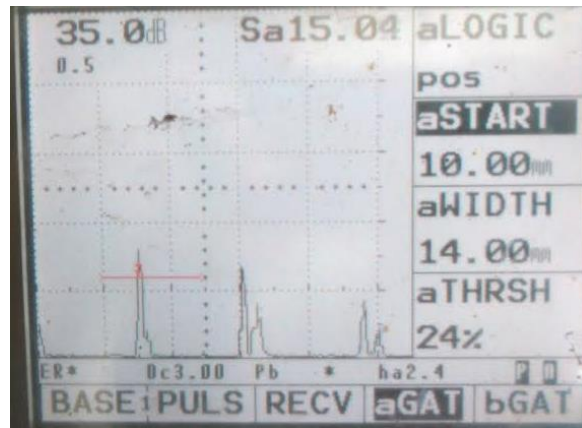


Figure 4.53: UT spectre for the Aluminium test vs. X-Ray part 1A

The aluminium part reveals a defect free structure, as seen in Figure 4.53, the X-ray do not show any defects on the structure and the US spectre shows the repetition of echoes due to the multiple reflections.

In summary, the use of NDT in AM parts can be resumed in the following main conclusions:

- UT technique proved a reliable technique in both materials to inspect defects in volume. This method, using the pulsed echo technique, is capable to detect defects in volume through the AM part, although:
 - The UT techniques are developed nowadays to analyse parts with high thicknesses;
 - UT equipment it is pretty simple but the major obstacle during these tests was the lack of records to analyse data after the scan;
- Phased Array Ultrasound testing revealed an excellent first iteration with potential to be studied in different conditions and compared to the other test methods ;
- The defects found were confirmed except the cases when the defects appear on the UT spectres and do not appear in the X-Ray film, due to the low film resolution considering that the IQI was indicated for those cases.

These tests that were performed confirm that UT pulsed echo technique is a feasible solution to analyse AM parts.

5. Conclusions

Additive Manufacturing of Aluminium alloy 5083 components, using CMT process, has been developed during this work. The proposed objectives were achieved and the main conclusions carried are:

1. All tested parameters were able for AM purposes, meaning, all parameters were good to produce wall build ups;
2. The deposition efficiency varies between 85.82% and 76.04%, considering that:
 - 2.1. Number of layers necessary to build up a wall is lower when the Current is higher;
 - 2.2. The deposition efficiency and the heat input present a quadratic behaviour due to the transfer modes associated to the MIG/MAG process, and the minimum value of deposition efficiency occurs on the current range that corresponds to the short circuit-spray transfer region;
3. The Useful mass ratio study reveals that best conditions for the best results in this study are 100A of current, approximately 148J/mm, 81% of deposition efficiency and 24 layers for the stipulated height of the wall build up;
 - 3.1. The number of layers, deposition efficiency and useful mass ration are directly dependent to the heat input of the process:
 - 3.1.1. Low heat input values are not enough to melt the material between layers and the poor fusion between layers implies more machining in the final product;
 - 3.1.2. High heat input is not recommended because the process stability is compromised and the metal transfer it is not so smooth;
4. The thermal cycle applied during the processing was not enough to ensure that the air cooling was sufficient to produce a fine grain microstructure and enhancing the mechanical properties. On the other hand, the hardness values obtained suggest two important aspects: improved ductility and homogeneous behaviour through all the wall section;
5. The porosity average size and distribution does not interfere significantly with the mechanical properties.
6. The Phased Array Testing and Ultrasonic Testing results were confirmed by the Radiation testing.

6.Future work

For future work, AM has a wide range of options like:

- Studying new materials with the electric arc welding equipment for AM purposes, as stainless steel for example;
- The corrosion resistance in AM parts is a subject relevant to study in the Aluminium 5083 alloy, mainly between layers;
- The metal forming techniques, as rolling, can be studied in order to improve mechanical properties in the aluminium AM walls;
- Try to produce different shapes, like a sphere, per example;
- Extensive study on NDT dedicated only for AM.

XI. References

1. Alcisto, J., Enriquez, A., Garcia, H., Hinkson, S., Steelman, T., Silverman, E., Valdovino, P., Gigerenzer, H., Foyos, J., Ogren, J., Dorey, J., Karg, K., McDonald, T. and Es-Said, O. (2010). Tensile Properties and Microstructures of Laser-Formed Ti-6Al-4V. *Journal of Materials Engineering and Performance*, 20(2), pp.203-212
2. Kruth, J., Leu, M. and Nakagawa, T. (1998). Progress in Additive Manufacturing and Rapid Prototyping. *CIRP Annals - Manufacturing Technology*, 47(2), pp.525-540
3. Levy, G., Schindel, R. and Kruth, J. (2003). RAPID MANUFACTURING AND RAPID TOOLING WITH LAYER MANUFACTURING (LM) TECHNOLOGIES, STATE OF THE ART AND FUTURE PERSPECTIVES. *CIRP Annals - Manufacturing Technology*, 52(2), pp.589-609
4. Roland Berger, (2013). *Additive Manufacturing, A game changer for the manufacturing industry?*. Munich
5. Mellor, S., Hao, L. and Zhang, D. (2013). Additive manufacturing: A framework for implementation. *Elsevier*, pp.1 – 2
6. Arcella, F. G. and Froes, F. H. (2000), Producing titanium aerospace components from powder using laser forming, *Journal of Minerals, Metals and Materials Society*, 52(5), p. 28-30.
7. Sequeira Almeida, P. (2012). *PROCESS CONTROL AND DEVELOPMENT IN WIRE AND ARC ADDITIVE MANUFACTURING*. PhD. Cranfield University.
8. Le Bourhis, F., Kerbrat, O., Dembinski, L., Hascoet, J. and Mognol, P. (2014). Predictive Model for Environmental Assessment in Additive Manufacturing Process. *Procedia CIRP*, 15, pp.26-31.
9. Sreenivasan, R., Goel, A. and Bourell, D. (2010). Sustainability issues in laser-based additive manufacturing. *Physics Procedia*, 5, pp.81-90
10. Pereira, M., Williams, M. and Du Preez, W. (2011). APPLICATION OF LASER ADDITIVE MANUFACTURING TO PRODUCE DIES FOR ALUMINIUM HIGH PRESSURE DIE-CASTING. *The South African Journal of Industrial Engineering*, 23(2).
11. Zhai, Yuwei, Diana A. Lados, and Jane L. Lagoy. "Additive Manufacturing: Making Imagination the Major Limitation." *The Minerals, Metals and Materials Society* 66.5 (2014)
12. Achilles, Ch., D. Aidonis, E. Iakovou, M. Thyaminidis, and D. Tzetzis. "A Methodological Framework for the Inclusion of Modern Additive Manufacturing into the Production Portfolio of a Focused Factory." *Journal of Manufacturing Systems*(2014)
13. Kruth, J. P., Levy, G., Klocke, F. and Childs, T. H. C. (2007), Consolidation phenomena in laser and powder-bed based layered manufacturing, *CIRP Annals - Manufacturing Technology*, 56(2), p. 730-759.
14. Gu, D., Meiners, W., Wissenbach, K. and Poprawe, R. (2012). Laser additive manufacturing of metallic components: materials, processes and mechanisms. *International Materials Review*, 57(3), pp.133-164.
15. Froes, F. H., Eylon, D., Eichelman, G. E. and Burte, H. M. (1980), Developments in titanium powder metallurgy, *Journal of Metals*, 32(2), p. 47-54
16. Groneck, D. and Harmon, D. (2003), Design development of unitized titanium structure, *Journal of Engineering for Gas Turbines and Power*, 125(1), p. 252-256
17. Messler, R. (1999). Principles of welding. New York: John Wiley.
18. Frazier, W. (2014). Metal Additive Manufacturing: A Review. *Journal of Materials Engineering and Performance*, 23(6), pp.1917-1928
19. Kruth, J. (1991). Material Incess Manufacturing by Rapid Prototyping Techniques. *CIRP Annals - Manufacturing Technology*, 40(2), pp.603-614
20. Karunakaran, K., Suryakumar, S., Pushpa, V. and Akula, S. (2010). Low cost integration of additive and subtractive processes for hybrid layered manufacturing. *Robotics and Computer-Integrated Manufacturing*, 26(5), pp. 490-499

21. Murr, Lawrence E., Edwin Martinez, Krista N. Amato, Sara M. Gaytan, Jennifer Hernandez, Diana A. Ramirez, Patrick W. Shindo, Frank Medina, and Ryan B. Wicker. "Fabrication of Metal and Alloy Components by Additive Manufacturing: Examples of 3D Materials Science." *Journal of Materials Research and Technology* 1.1 (2012): 42-54
22. Wong, K. and Hernandez, A. (2012). A Review of Additive Manufacturing. *ISRN Mechanical Engineering*, 2012, pp.1-10
23. Suo, H., Chen, Z., Liu, J., Gong, S. and Xiao, J. (2014). Microstructure and Mechanical Properties of Ti-6Al-4V by Electron Beam Rapid Manufacturing. *Rare Metal Materials and Engineering*, 43(4), pp.780-785
24. Murr, Lawrence E., Sara M. Gaytan, Diana A. Ramirez, Edwin Martinez, Jennifer Hernandez, Krista N. Amato, Patrick W. Shindo, Francisco R. Medina, and Ryan B. Wicker. "Metal Fabrication by Additive Manufacturing Using Laser and Electron Beam Melting Technologies." *Journal of Materials Science & Technology* 28.1 (2012): 1-14
25. M. Ghazy, M. (2012). *Development of an Additive Manufacturing Decision Support System (AMDSS)*. PhD. School of Mechanical and Systems Engineering Newcastle University.
26. Tamingir, K. M. and Hafley, R. A. (2006), "Electron beam freeform fabrication for cost effective near-net shape manufacturing", NATO/RTOAVT- 139 (Specialists' meeting on cost effective manufacture via net shape processing), Amsterdam
27. Das, S., Beaman, J. J. and Bourell, M. W. D. L. (1998a), Direct laser freeform fabrication of high performance metal components, *Rapid Prototyping Journal*, 4(3), p. 112-117.
28. Vayre, B., F. Vignat, and F. Villeneuve. "Identification on Some Design Key Parameters for Additive Manufacturing: Application on Electron Beam Melting." *Procedia CIRP* 7 (2013): 264-69
29. Brandl, Erhard, Frank Palm, Vesselin Michailov, Bernd Viehweger, and Christoph Leyens. "Mechanical Properties of Additive Manufactured Titanium (Ti-6Al-4V) Blocks Deposited by a Solid-state Laser and Wire." *Materials & Design* 32.10 (2011): 4665-675
30. Saqib, S., Urbanic, R. and Aggarwal, K. (2014). Analysis of Laser Cladding Bead Morphology for Developing Additive Manufacturing Travel Paths. *Procedia CIRP*, 17, pp.824-829
31. Levy, G. (2010). The role and future of the Laser Technology in the Additive Manufacturing environment. *Physics Procedia*, 5, pp.65-80
32. Das, S., Wohler, M., Beaman, J. J. and Bourell, D. L. (1999), Processing of titanium net shapes by SLS/HIP, *Materials and Design*, 20(2-3), p. 115-121
33. Tamingir, K. M. and Hafley, R. A. (2003), Electron beam freeform fabrication: A rapid metal deposition in: *Proceedings of the 3rd Annual Automotive Composites Conference (Society of Plastic Engineers SPE)*, September 9-10th, Troy, MI, USA, p. 1-6
34. Vilar, R. (1999), Laser cladding, *Journal of Laser Applications*, 11(2), p. 64-79
35. Pinkerton, A. J., Syed, W. U. H. and Li, L. (2007), Theoretical analysis of the coincident wire-powder laser deposition process, *Journal of Manufacturing Science and Engineering*
36. Kumar, S. and Pityana, S. (2011). Laser-Based Additive Manufacturing of Metals. *AMR*, 227, pp.92-95.
37. Levy, G. N., Schindel, R. and Kruth, J. P. (2003), "RAPID MANUFACTURING AND RAPID TOOLING WITH LAYER MANUFACTURING (LM) TECHNOLOGIES, STATE OF THE ART AND FUTURE PERSPECTIVES", *CIRP Annals - Manufacturing Technology*, vol. 52, no. 2, pp. 589-609
38. Santos, E. C., Shiomi, M., Osakada, K. and Laoui, T. (2006), "Rapid manufacturing of metal components by laser forming", *International Journal of Machine Tools and Manufacture*, vol. 46, no. 12-13, pp. 1459-1468
39. Marya, S., Hascoet, J., Panigrahy, S., Marya, M. and Singh, V. (2014). *Additive manufacturing, derivative of welding & joining technology- A literature review*.
40. Li, Y. and Gu, D. (2014). Parametric analysis of thermal behavior during selective laser melting additive manufacturing of aluminum alloy powder. *Materials & Design*, 63, pp.856-867.
41. Unocic, R. and DuPont, J. (2004). Process efficiency measurements in the laser engineered net shaping process. *Metallurgical and Materials Transactions B*, 35(1), pp.143-152

42. Baufeld, B., Biest, O. V. d. and Gault, R. (2010), "Additive manufacturing of Ti-6Al-4V components by shaped metal deposition: Microstructure and mechanical properties", *Materials & Design*, vol. 31, Supplement 1, no. 0, pp. 106-111
43. Xiong, J. and Zhang, G. (2014). Adaptive control of deposited height in GMAW-based layer additive manufacturing. *Journal of Materials Processing Technology*, 214(4), pp.962-968
44. Pinkerton, A. and Li, L. (2004). Direct additive laser manufacturing using gas- and water-atomised H13 tool steel powders. *Int J Adv Manuf Technol*, 25 (5-6), pp.471-479.
45. Alberti, E., Silva, L. and d'Oliveira, A. (2014). Manufatura Aditiva: o papel da soldagem nesta janela de oportunidade. *Soldag. insp.*, 19(2), pp.190-198
46. Baker, R., Westinghouse Electric & Manufacturing Company (1925), *Method of making decorative articles*, United States Patent No.1,533,300
47. Martina, F., Mehnen, J., Williams, S., Colegrove, P. and Wang, F. (2012). Investigation of the benefits of plasma deposition for the additive layer manufacture of Ti-6Al-4V. *Journal of Materials Processing Technology*, 212(6), pp.1377-1386
48. Baufeld, B., Brandl, E. and van der Biest, O. (2011). Wire based additive layer manufacturing: Comparison of microstructure and mechanical properties of Ti-6Al-4V components fabricated by laser-beam deposition and shaped metal deposition. *Journal of Materials Processing Technology*, 211(6), pp.1146-1158
49. Xiong, J. and Zhang, G. (2014). Adaptive control of deposited height in GMAW-based layer additive manufacturing. *Journal of Materials Processing Technology*, 214(4), pp.962-968
50. Ding, D., Pan, Z., Cuiuri, D. and Li, H. (2015). A multi-bead overlapping model for robotic wire and arc additive manufacturing (WAAM). *Robotics and Computer-Integrated Manufacturing*, 31, pp.101-110.
51. F. Oliveira Santos, J. and Quintino, L. (n.d.). *Processos de Soldadura*. 2nd ed. Oeiras: Instituto de Soldadura e Qualidade
52. Quintino, L. (2010). *Processos de Ligação: Apresentações das aulas*.
53. Rosado, T. (n.d.). Innovation in the MIG/MAG process: productivity analysis and fume emissions
54. Substech.com, (2014). *Metal Inert Gas Welding (MIG, GMAW) [SubsTech]*. [online] Available at: http://www.substech.com/dokuwiki/doku.php?id=metal_inert_gas_welding_mig_gmaw [Accessed 1 Nov. 2014].
55. Inc., P. (2014). *Cold Metal Transfer: Seam Welding*. [online] Protocase.com. Available at: http://www.protocase.com/products/mcf_seam_welding.php [Accessed 2 Nov. 2014]
56. Zhu, Y., Li, J., Tian, X., Wang, H. and Liu, D. (2014). Microstructure and mechanical properties of hybrid fabricated Ti-6.5Al-3.5Mo-1.5Zr-0.3Si titanium alloy by laser additive manufacturing. *Materials Science and Engineering: A*, 607, pp.427-434.
57. Wycisk, E., Solbach, A., Siddique, S., Herzog, D., Walther, F. and Emmelmann, C. (2014). Effects of Defects in Laser Additive Manufactured Ti-6Al-4V on Fatigue Properties. *Physics Procedia*, 56, pp.371-378.
58. Cooper, D., Stanford, M., Kibble, K. and Gibbons, G. (2012). Additive Manufacturing for product improvement at Red Bull Technology. *Materials & Design*, 41, pp.226-230.
59. Wang, F., Mei, J., Jiang, H. and Wu, X. (2007). Laser fabrication of Ti6Al4V/TiC composites using simultaneous powder and wire feed. *Materials Science and Engineering: A*, 445-446, pp.461-466.
60. Denlinger, E., Heigel, J., Michaleris, P. and Palmer, T. (2015). Effect of inter-layer dwell time on distortion and residual stress in additive manufacturing of titanium and nickel alloys. *Journal of Materials Processing Technology*, 215, pp.123-131.
61. Syed, W., Pinkerton, A. and Li, L. (2006). Combining wire and coaxial powder feeding in laser direct metal deposition for rapid prototyping. *Applied Surface Science*, 252(13), pp.4803-4808.

62. Schmidtke, K., Palm, F., Hawkins, A. and Emmelmann, C. (2011). Process and Mechanical Properties: Applicability of a Scandium modified Al-alloy for Laser Additive Manufacturing. *Physics Procedia*, 12, pp.369-374.
63. Jhavar, S., Jain, N. and Paul, C. (2014). Development of micro-plasma transferred arc (μ -PTA) wire deposition process for additive layer manufacturing applications. *Journal of Materials Processing Technology*, 214(5), pp.1102-1110.
64. Wanjara, P., Brochu, M. and Jahazi, M. (2007). Electron beam freeforming of stainless steel using solid wire feed. *Materials & Design*, 28(8), pp.2278-2286.
65. King, W., Barth, H., Castillo, V., Gallegos, G., Gibbs, J., Hahn, D., Kamath, C. and Rubenchik, A. (2014). Observation of keyhole-mode laser melting in laser powder-bed fusion additive manufacturing. *Journal of Materials Processing Technology*, 214(12), pp.2915-2925.
66. Jia, Q. and Gu, D. (2014). Selective laser melting additive manufacturing of Inconel 718 superalloy parts: Densification, microstructure and properties. *Journal of Alloys and Compounds*, 585, pp.713-721.
67. Dehoff, R. and Babu, S. (2010). Characterization of interfacial microstructures in 3003 aluminum alloy blocks fabricated by ultrasonic additive manufacturing. *Acta Materialia*, 58(13), pp.4305-4315.
68. Shimizu, S., Fujii, H., Sato, Y., Kokawa, H., Sriraman, M. and Babu, S. (2014). Mechanism of weld formation during very-high-power ultrasonic additive manufacturing of Al alloy 6061. *Acta Materialia*, 74, pp.234-243.
69. Liang, Y., Liu, D. and Wang, H. (2014). Microstructure and mechanical behavior of commercial purity Ti/Ti-6Al-2Zr-1Mo-1V structurally graded material fabricated by laser additive manufacturing. *Scripta Materialia*, 74, pp.80-83.
70. Järvinen, J., Matilainen, V., Li, X., Piili, H., Salminen, A., Mäkelä, I. and Nyrhilä, O. (2014). Characterization of Effect of Support Structures in Laser Additive Manufacturing of Stainless Steel. *Physics Procedia*, 56, pp.72-81.
71. Suo, H., Chen, Z., Liu, J., Gong, S. and Xiao, J. (2014). Microstructure and Mechanical Properties of Ti-6Al-4V by Electron Beam Rapid Manufacturing. *Rare Metal Materials and Engineering*, 43(4), pp.780-785.
72. Pinkerton, A. and Li, L. (2004). Direct additive laser manufacturing using gas- and water-atomised H13 tool steel powders. *Int J Adv Manuf Technol*, 25(5-6), pp.471-479.
73. Casalino, G., Campanelli, S. and Ludovico, A. (2013). Laser-arc hybrid welding of wrought to selective laser molten stainless steel. *Int J Adv Manuf Technol*, 68(1-4), pp.209-216.
74. Wu, A., Brown, D., Kumar, M., Gallegos, G. and King, W. (2014). An Experimental Investigation into Additive Manufacturing-Induced Residual Stresses in 316L Stainless Steel. *Metall and Mat Trans A*, 45(13), pp.6260-6270.
75. Baufeld, B., Biest, O., Gault, R. and Ridgway, K. (2011). Manufacturing Ti-6Al-4V Components by Shaped Metal Deposition: Microstructure and Mechanical Properties. *IOP Conference Series: Materials Science and Engineering*, 26, p.012001.
76. Clark, D., Bache, M. and Whittaker, M. (2008). Shaped metal deposition of a nickel alloy for aero engine applications. *Journal of Materials Processing Technology*, 203(1-3), pp.439-448.
77. Wang, F., Williams, S. and Rush, M. (2011). Morphology investigation on direct current pulsed gas tungsten arc welded additive layer manufactured Ti6Al4V alloy. *Int J Adv Manuf Technol*, 57(5-8), pp.597-603.
78. Baufeld, B. (2011). Mechanical Properties of INCONEL 718 Parts Manufactured by Shaped Metal Deposition (SMD). *Journal of Materials Engineering and Performance*, 21(7), pp.1416-1421.
79. Edwards, P., O'Conner, A., and Ramulu, M., 2013, "Electron Beam Additive Manufacturing of Titanium Components: Properties and Performance," *ASME J. Manuf. Sci. Eng.*, 135(6), p. 061016.

80. Kruth, J.-P., Mercelis, P., Van Vaerenbergh, J., and Craeghs, T., 2007, "Feedback Control of Selective Laser Melting," Proceedings of the 3rd International Conference on Advanced Research in Virtual and Rapid Prototyping, Leiria, Portugal, Sept. 24–29, pp. 521–527.
81. Jamshidinia, M., Kong, F., and Kovacevic, R., 2013, "Numerical Modeling of Heat Distribution in the Electron Beam Melting of Ti–6Al–4V," ASME J.Manuf. Sci. Eng., 135(6), p. 061010.
82. Fischer, P., Locher, M., Romano, V., Weber, H.-P., Kolossov, S., and Glardon, R., 2004, "Temperature Measurements During Selective Laser Sintering of Titanium Powder," Int. J. Mach. Tools Manuf., 44(12), pp.1293–1296
83. Shah, K., Pinkerton, A. J., Salman, A., and Li, L., 2010, "Effects of Melt Pool Variables and Process Parameters in Laser Direct Metal Deposition of Aerospace Alloys," Mater. Manuf. Process., 25(12), pp. 1372–1380.
84. Qian, L., Mei, J., Liang, J., and Wu, X., 2005, "Influence of Position and Laser Power on Thermal History and Microstructure of Direct Laser Fabricated Ti–6Al–4V Samples," Mater. Sci. Technol., 21(5), pp. 597–605.
85. Zhong, M., Liu, W., Ning, G., Yang, L., and Chen, Y., 2004, "Laser Direct Manufacturing of Tungsten Nickel Collimation Component," J. Mater. Process. Technol., 147(2), pp. 167–173.
86. Labudovic, M., Hu, D., and Kovacevic, R., 2003, "A Three Dimensional Model for Direct Laser Metal Powder Deposition and Rapid Prototyping," J.Mater. Sci., 38(1), pp. 35–49.
87. Islam, M., Purtonen, T., Piili, H., Salminen, A., and Nyrhilä, O., 2013, "Temperature Profile and Imaging Analysis of Laser Additive Manufacturing of Stainless Steel," Phys. Procedia, 41, pp. 828–835.
88. Dadbakhsh, S., Hao, L., and Sewell, N., 2012, "Effect of Selective Laser Melting Layout on the Quality of Stainless Steel Parts," Rapid Prototyping J., 18(3), pp. 241–249.
89. Childs, T., Hauser, C., and Badrossamay, M., 2005, "Selective Laser Sintering (Melting) of Stainless and Tool Steel Powders: Experiments and Modeling," Proc. Inst. Mech. Eng., Part B, 219(4), pp. 339–357.
90. Hofmeister, W., and Griffith, M., 2001, "Solidification in Direct Metal Deposition by LENS Processing," JOM, 53(9), pp. 30–34.
91. Clare, A., Oyelola, O., Abioye, T., and Farayibi, P., 2012, "Laser Cladding of Rail Steel with Co–Cr," Proceedings of the 37th International MATADOR Conference, Vol. 10, pp. 349–353.
92. Hu, Y., Chen, C., and Mukherjee, K., 2000, "Measurement of Temperature Distributions during Laser Cladding Process," J. Laser Appl., 12(3), pp.126–130.
93. Toyserkani, E., and Khajepour, A., 2006, "A Mechatronics Approach to Laser Powder Deposition Process," Mechatronics, 16(10), pp. 631–641.
94. Kelly, G. S., Advani, S. G., Gillespie, J. W., Jr., and Bogetti, T. A., 2013, "A Model to Characterize Acoustic Softening During Ultrasonic Consolidation," J. Mater. Process. Technol., 213(11), pp. 1835–1845.
95. Sriraman, M., Gonser, M., Fujii, H. T., Babu, S., and Bloss, M., 2011, "Thermal Transients During Processing of Materials by Very High Power Ultrasonic Additive Manufacturing," J. Mater. Process. Technol., 211(10), pp.1650–1657.
96. Song, Y.-A., and Koenig, W., 1997, "Experimental Study of the Basic Process Mechanism for Direct Selective Laser Sintering of Low-Melting Metallic Powder," CIRP Ann. Manuf. Technol., 46(1), pp. 127–130.
97. Light Alloys - Metallurgy of the Light Metals, I. J. Polmear, 1995, Edward Arnold, 3^a Ed.;
98. Ferro, A. (2010). *Materiais Metálicos: Apresentações das aulas*.
99. Twi-global.com, (2015). MIG/MAG – developments in low heat input transfer modes. [online] Available at: <http://www.twi-global.com/technical-knowledge/job-knowledge/mig-mag-developments-in-low-heat-input-transfer-modes-133/> [Accessed 21 Apr. 2015].
100. O'Brien, R L. *Welding Handbook*. Miami, Fla.: American Welding Society, 1991. Print.
101. Esabna.com,. 'Handbook - Metal Transfer Variations'. N.p., 2015. Web. 24 Apr. 2015.
102. Twi-global.com,. 'MIG/MAG – Developments In Low Heat Input Transfer Modes'. N.p., 2015. Web. 25 Apr. 2015.
103. Nde-ed.org, (2015). Introduction to Ultrasonic Testing. [online] Available at: <https://www.nde-ed.org/EducationResources/CommunityCollege/Ultrasonics/Introduction/description.htm> [Accessed 15 Sep. 2015].

104. Sá Nogueira, A. (2013). Phased Array test procedure usable in detection of flaws existing on groove surface of high thickness narrow gap welding. Master Degree. Instituto Superior Técnico.
105. Pickin, C.G., Williams, S.W, M.L., 2011. Characterisation of the cold metal transfer (CMT) process and its application for low dilution cladding. , 211(3), pp.496–502.
106. Matweb.com, (2015). MatWeb - The Online Materials Information Resource. [online] Available at:
<http://www.matweb.com/search/DataSheet.aspx?MatGUID=d105c2a24d6942cdad79259f770fb806&ckck=1> [Accessed 1 Oct. 2015].
107. Palani, P. K., & Murugan, N. (2006). Selection of parameters of pulsed current gas metal arc welding. *Journal of Materials Processing Technology*, 172, 1–10.
108. Kang, J. G., Ryu, G. S., Kim, D. C., Kang, M. J., Park, Y. W., & Rhee, S. (2013). Optimization of arc-start performance by wire-feeding control for GMA welding. *Journal of Mechanical Science and Technology*, 27(2), 501–509..
109. Gungor, Beytullah et al. 'Mechanical And Microstructural Properties Of Robotic Cold Metal Transfer (CMT) Welded 5083-H111 And 6082-T651 Aluminum Alloys'. *Materials & Design* 54 (2014): 207-211. Web.
110. Norma ASTM E 112-88, "Standard test methods for determining average grain size";
111. Arc welding of Non Ferrous metals. (2015). 1st ed. Tokyo: Kobe Steel Ltd.
112. Kieppura, Robert T.; Sanders, Bonnie R.; *Metals Handbook – Metallography and microstructures*; volume 8; 9ª edição; American society for metals; 1985.

XII. Appendixes

Appendix A: Technical Specification Sheet of Filler wire ER5356



T H E H A R R I S P R O D U C T S G R O U P
A L I N C O L N E L E C T R I C C O M P A N Y
 4501 Quality Place • Mason, OH 45040 U.S.A Tel: 513-754-2000 Fax: 513-754-6015
TECHNICAL SPECIFICATION SHEET

5356 ALUMINUM WELD WIRE

STATEMENT OF LIABILITY- DISCLAIMER

Any suggestion of product applications or results is given without representation or warranty, either expressed or implied. Without exception or limitation, there are no warranties of merchantability or of fitness for particular purpose or application. The user must fully evaluate every process and application in all aspects, including suitability, compliance with applicable law and non-infringement of the rights of others. The Harris Products Group and its affiliates shall have no liability in respect thereof.

NOMINAL COMPOSITION:

Aluminum	BALANCE	Titanium	.06-.20 %
Magnesium	4.5-5.5 %	Copper	.10 % max.
Manganese	.05-.20 %	Chromium	.05-.20 %
Silicon	.25 % max.	Zinc	.10 % max.
Beryllium	.0008 % max.	Iron	.40% max.
Others	Each .05% max. Total .15 % max.		

PHYSICAL PROPERTIES:

Solidus	1060 °F (571 °C)	Density lbs/cu in	.096
Liquidus	1175 °F (635 °C)	Post Anodize Color	White
As Welded Base Plate of 5086			
Tensile Strength	39,000 psi	Elongation in 2"	17%
Yield Strength	19,000 psi		

RECOMMENDED WELDING PARAMETERS:

* GMAW (MIG) Parameters (DC Reverse Polarity) Electrode Positive Spray transfer

Metal Thickness	Wire Diameter	Amps	Volts	Argon
1/16"	.030	70-110	15-20	25
1/8"	.030-3/64	120-150	20-24	30
3/16"	.030-3/64	130-210	22-26	30-35
1/4"	3/64-1/16	170-225	24-28	40
3/8"	1/16	225-300	26-29	50

*GTAW (TIG) Parameters (AC) Hemisphere tip shape tungsten electrode

Metal (1)	Pure or zirconiated	Filler Wire Size	Amps	Volts ACHF	Gas Cup	Argon (cfh)
1/16"	1/16"- 3/32"	1/16"-3/32"	70-100	15	3/8	20
1/8"	1/8"-5/32"	1/8"-5/32"	125-175	15	7/16	20
3/16"	5/32"-3/16"	5/32-3/16"	170-225	15	7/16-1/2	25
1/4"	3/16"-1/4"	3/16"	220-275	15	1/2	30
3/8"	1/4"	3/16"-1/4"	330-380	15	5/8	35
1/2"	1/4"	1/4"	400-450	25	5/8	35

All statements, information and data given are believed to be accurate and reliable but are presented without guarantee, warranty or responsibility of any kind, expressed or implied.

Additional information available at our web site: www.harrisproductsgroup.com

Appendix B: Experimental Procedure for Metallographic analysis

Appendix B1: Experimental procedure for Macrostructure and analysis

The procedure followed for the sample preparation and posterior macrostructure analysis was:

- 1) Cutting the samples and deburr before mounting samples;
- 2) Identify all the samples according to the test part to analyse by mechanical engraving;
- 3) Use epoxy resin to mount the samples;
- 4) Proceed to grinding operations using wet sandpaper, following this mesh size for the sandpaper: 600, 800, 1200 and 2400;
- 5) Proceed to polishing operation by using polishing cloths oiled with the proper lubricant and the diamond polishing colloidal solution, following the granulometry of: 3 μ m, 1 μ m and 0.6 μ m. Between granulometries it is recommended to wash vigorously the cloths with soap and water, and proceed to the sample cleaning without direct contact, like ultrasound cleaning per example.
- 6) Image capturing and editing, in order to obtain the correct scale to analyse the macrostructure.

Appendix B2: Experimental procedure for Microstructure and analysis

- 1) Cutting the samples and deburr before mounting samples;
- 2) Identify all the samples according to the test part to analyse by mechanical engraving;
- 3) Use epoxy resin to mount the samples;
- 4) Proceed to grinding operations using wet sandpaper, following this mesh size for the sandpaper: 600, 800, 1200 and 2400. The sandpapers should be only used for aluminium alloy grinding;
- 5) Proceed to polishing operation by using polishing cloths oiled with the proper lubricant and the diamond polishing colloidal solution, following the granulometry of: 3 μ m, 1 μ m and 0.6 μ m. Between granulometries it is recommended to wash vigorously the cloths with soap and water, and proceed to the sample cleaning without direct contact, like ultrasound cleaning per example. The polishing cloths should be used only for aluminium alloys
- 6) If the samples present scratches or other irregularities, repeat step 4);
- 7) Etching operation with Keller solution, the sample is emerged in the Keller solution time enough until the microstructure is revealed. In alternative, the Modified Poulton solution can be used but the time of immersion should be inferior to the Keller solution due to the reactivity of Modified Poulton solution. The time for etching is typical 20s for Keller solution and 5s for Modified Poulton solution. The following tables reveal the chemical compositions for both solutions [112]:

Keller solution composition
2mL of HF
3mL of HCl
5mL of HNO ₃
190mL of H ₂ O

Modified Poulton solution
50mL of Poulton solution
25mL of HNO ₃
40mL of solution in which for every 10 ml of H ₂ O joins 3g chromic acid

Poulton Solution
12mL of HCl
6mL of HNO ₃
1mL of HF
1mL of H ₂ O

- 8) Capture microstructure images and analyse the results.

Appendix C: Experimental Procedure for Hardness testing

The test procedure adopted for Hardness tests of the AM wall sections was the following:

- 1) Calculate the distance between the bottom and the top of the section;
- 2) Estimate the average high value of the diagonal possible to obtain;
- 3) Establish an indentation plan according to the sample to be tested, in this case the spacemete between indentations was 1mm across all section;
- 4) Program the durometer *Struers -1/-2* with the load value of 4.902N, 15s of indentation time and the number of indentations;
- 5) Set the sample position and adjust with the 20x in order to adjust the central position and the direction of measuring;
- 6) Change the lens for the identer and start de indentation process;
- 7) After each test, change again to the 20x lens and measure both diagonals;
- 8) Read and save the measured value;
- 9) If there is more samples to test, repeat the procedure after step 6), included that one.

Appendix C1: Values obtained of Hardness testing

60A		80A		110A		130A	
AM wall height (mm)	Hardness (HV)	AM wall height (mm)	Hardness (HV)	AM wall height (mm)	Hardness (HV)	AM wall height (mm)	Hardness (HV)
1	67,9	1	63,6	1	63,7	1	63,5
2	68,5	2	68,4	2	60,3	2	62,9
3	66,7	3	68,9	3	62,3	3	55,1
4	61,3	4	64,9	4	65,1	4	60,2
5	62,2	5	69,8	5	68,7	5	64,2
6	62,8	6	64,4	6	64,7	6	61,8
7	61,4	7	68,5	7	62,9	7	62,5
8	66,4	8	66,7	8	54,2	8	65,1
9	68,9	9	69,5	9	61,1	9	59,5
10	65,1	10	65,1	10	58,4	10	64,6
11	65,7	11	70	11	57,9	11	64,7
12	64,7	12	67,2	12	59,7	12	55,3
13	65,9	13	69,5	13	64,5	13	58,3
14	65	14	77	14	59,9	14	61,4
15	62,4	15	69,5	15	66,3	15	52,5
16	65	16	69,1	16	68	16	59,4
17	66,2	17	69,6	17	59,3	17	58,3
18	63	18	58,7	18	61,9	18	67,4
19	68	19	65,9	19	60,2	19	60,1
20	65,1	20	61,3	20	67,3	20	58,5
21	63,6	21	59,7	21	60,4	21	59,3
22	64,6	22	65,5	22	59,4	22	60,4
23	69,9	23	63,3	23	53,4	23	54,8
24	64,8	24	59,9	24	58,2	24	62,8
25	63,7	25	60	25	61	25	59,9